JACS
JOURNAL OF THE AMERICAN CHEMICAL SOCIETY
pubs.acs.org/JACS
Article

Exploring Host−Guest Interactions within a 600 kDa DegP Protease Cage Complex Using Hydrodynamics Measurements and Methyl-TROSY NMR

Robert W. Harkness,* Huaying Zhao, Yuki Toyama, Peter Schuck, and Lewis E. Kay*

Cite This: J. Am. Chem. Soc. 2024, 146, 8242−8259
Read Online
ACCESS | Metrics & More | Article Recommendations | Supporting Information

ABSTRACT: The DegP protease-chaperone operates within the periplasm of Gram-negative bacteria, where it assists in the regulation of protein homeostasis, promotes virulence, and is essential to survival under stress. To carry out these tasks, DegP forms a network of preorganized apo oligomers that facilitate the capture of substrates within distributions of cage-like complexes which expand to encapsulate clients of various sizes. Although the architectures of DegP cage complexes are well understood, little is known about the structures, dynamics, and interactions of client proteins within DegP cages and the relationship between client structural dynamics and function. Here, we probe host−guest interactions within a 600 kDa DegP cage complex throughout the DegP activation cycle using a model α-helical client protein through a combination of hydrodynamics measurements, methyl-transverse relaxation optimized spectroscopy-based solution nuclear magnetic resonance studies, and proteolytic activity assays. We find that in the presence of the client, DegP cages assemble cooperatively with few intermediates. Our data further show that the N-terminal half of the bound client, which projects into the interior of the cages, is predominantly unfolded and flexible, and exchanges between multiple conformational states over a wide range of time scales. Finally, we show that a concerted structural transition of the protease domains of DegP occurs upon client engagement, leading to activation. Together, our findings support a model of DegP as a highly cooperative and dynamic molecular machine that stabilizes unfolded states of clients, primarily via interactions with their C-termini, giving rise to efficient cleavage.

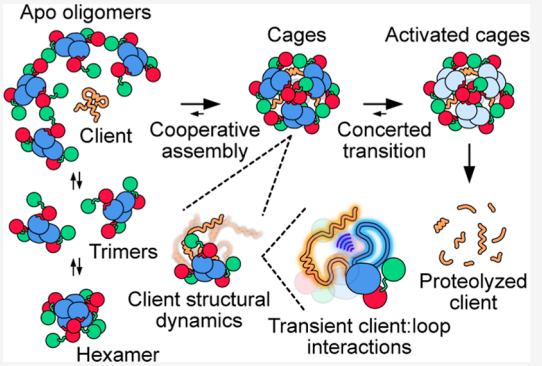

1. INTRODUCTION

Living organisms depend upon molecular "machines" that maintain protein homeostasis in order to ensure proper cellular function.[1,2] These machines, in the form of protein chaperones[3,4] and proteases,[5,6] make up a tightly regulated nexus which establishes the appropriate folding and localization of cellular proteins or their recycling when they are no longer needed. Impairment of this quality control system leads to the misfolding and aggregation of protein molecules[7] which, in turn, gives rise to cellular dysfunction and in severe cases cell death.[8] The high-temperature requirement A (HtrA) protein family,[9−11] conserved from bacteria to mammals, consists of key proteases that degrade misfolded proteins. Under some conditions, members of the family can also function as chaperones and thus exhibit dual functionality.[9] HtrA proteins participate in the regulation of numerous signaling pathways including those involved in cell motility,[12] division,[13] and apoptosis,[14] highlighting their key role in cellular fitness.

DegP is a bacterial orthologue of the HtrA protein family that operates in the periplasm of Gram-negative bacteria,[15,16] some members of which form the antibiotic resistant group of ESKAPE pathogens that pose a serious threat to human health.[17] DegP serves in a stress-response role, as shown by its overexpression in reaction to heat and other forms of shock[18−20] and by the inability of DegP knockout cell lines to grow under stress conditions.[21] In addition to its general protective role in the periplasm, DegP is also an important contributor to bacterial pathogenicity through its participation in the export and recycling of bacterial virulence factors.[22−24] Virulence factors known to interact with DegP include autotransporters[25,26] and outer membrane proteins (OMPs)[27,28] which are involved in the degradation of host proteins and toxin export, respectively, among other virulence-promoting functions.

The basic functional units of DegP are trimers consisting of protomers comprised of a serine protease domain followed by two tandem PDZ domains[10] (PDZ1 and PDZ2, Figure 1A top). The protomers (UniProt residue numbering 1−474) initially carry an N-terminal periplasmic signal sequence

Received: November 25, 2023
Revised: February 25, 2024
Accepted: February 27, 2024
Published: March 13, 2024

https://doi.org/10.1021/jacs.3c13247
J. Am. Chem. Soc. 2024, 146, 8242−8259

(residues 1−26) that is removed upon entry to the periplasm, yielding the mature subunit (residues 27−474, hereafter renumbered as 1−448). The trimers are tightly assembled through interprotomer protease domain interactions, with the PDZ domains localized to the exteriors of the trimer particles (Figure 1A). A disordered region of the protease domains, referred to as the LA loops (residues 36−81, Figure 1B left), and the protease−PDZ1 and PDZ1−PDZ2 linker sequences, in addition to the inherent flexibility of the PDZ1 and PDZ2 domains, enable DegP to form a wide variety of higher-order oligomeric states (Figure 1A middle, Figure 1B left and middle) that are implicated in function.[10,28−31] Traditionally, DegP function was explained in terms of switching between an inactive, apo hexamer state where the LA loops from one trimer sequester the active sites of the opposing trimer[10] (Figure 1B left), and proteolytically active, cage-like 12mer and 24mer structures (Figure 1B middle). The PDZ1 and protease domain client binding sites in the "closed" apo hexamer structure (path A hexamer, often referred to as M_{6A} in what follows) are occluded, thus mitigating undesired substrate binding and proteolysis. M_{6A} was shown to be stabilized by intertrimer protease^{i}:protease^{j} and PDZ1^{i}:PDZ1^{j} domain interactions[10] (Figure 1B, left, i = 1, j = 2; in what follows the superscripted i and j indicate separate trimers, $i \neq j$). Further investigations of the DegP structure revealed a more complex energy landscape comprised of a large range of cage-like assemblies[18] that then reorganize upon client engagement (Figure 1A, middle and bottom) to form discrete complexes which are stabilized by PDZ1^{i}:PDZ2^{j} interactions (Figure 1B, middle).[29] These assemblies have been shown in some cases to hold clients or to promote their refolding via holdase-type activities, while in other situations, the bound substrate is proteolyzed.[9]

In recent investigations from our group, we have explored the energetics of DegP's self-assembly landscape in the absence and presence of model substrates under a variety of simulated physiological conditions so as to understand how cage remodeling is involved in the maintenance of protein homeostasis.[18,31] We demonstrated that in the absence of client proteins, the energy landscape of DegP rapidly changes in response to stress. The redistribution of the apo DegP ensemble could be described in terms of two pathways (Figure 1A, middle), one of which serves to buffer the concentration of free trimers through the formation of M_{6A} (path A, blue) and is predominantly operative at lower temperatures, while the other (path B, red) becomes active at higher temperatures and features the assembly of cage-like species mediated by relatively weakly associating and rapidly exchanging trimer units. Our studies[18,31] have revealed that M_{6A}, corresponding to the closed hexamer that was initially characterized via X-ray crystallography,[10] is not appreciably populated under conditions where bacteria grow efficiently (e.g., human host temperatures and salt concentrations) and therefore does not appear to play a major role in modulating the availability of trimers for engaging clients in these circumstances. Rather, the network of preorganized assemblies in path B underlies the formation of discrete cage complexes and shifts toward much larger species under stress conditions (e.g., heat shock and the associated overexpression of DegP[21]) to quickly capture clients.[18] Using a panel of engineered client proteins, we further showed that substrate-bound DegP forms distributions of expandable cage particles whose dimensions depend on the size of the substrate within the cage interiors.[31] Remarkably, these cage ensembles can include species with sizes up to subcellular organelles. Together, the rapid assembly and extraordinary structural plasticity of the DegP trimers enables the engagement of different types of clients in the periplasm.

Although we and others have established the architectures of DegP cage complexes,[10,28−31] less is known about the interactions between DegP and clients within cages, particularly for substrates that are well-structured in the unbound state, and whether these potential interactions influence the cooperativity of cage formation or proteolytic activation. This, in part, reflects the fact that relatively short, disordered substrates have typically been used in studies of DegP[32,33] as well as the difficulty in obtaining high-resolution structural maps of clients within DegP cages, likely due to the inherent dynamics of the complexes. For example, most studies exploring DegP:substrate interactions have used small peptides or fragments of proteins as model clients,[29,32,33] regions of which were not well-resolved in complex with DegP via X-ray crystallography, though partial density could be observed in the protease and PDZ1 domain binding sites. Similarly, electron cryo-microscopy (cryo-EM) studies exploiting larger, folded clients which could fill the cage interiors (e.g., OMPs) did not generate maps of sufficient resolution to accurately visualize the internalized substrate.[28] We recently showed via cryo-EM that the C-terminal half of a model α-helical client, the DNA binding domain of human telomere repeat binding factor 1[34] (hTRF1, Figure 1B right), retains folded structure within a 12mer cage.[31] We were, however, unable to obtain information on the N-terminal half of hTRF1 that projects into the cage interior and potentially forms interactions with the protease domain LA loops to modulate activity. Given that many clients of DegP are likely to be at least partly folded in their unbound state, it is of interest to gain insight into how such folded protein substrates promote cage formation and whether their structural dynamics and interactions within the interior of cages, including, potentially, with the unfolded LA loops, can influence proteolysis.

Here, we explore the influence of hTRF1 on the oligomeric landscape and activation mechanism of DegP, providing insights into host−guest interactions between the client and DegP within cages. Using a combination of analytical ultracentrifugation (AUC) and methyl-transverse relaxation optimized spectroscopy (methyl-TROSY)-based solution nuclear magnetic resonance (NMR) spectroscopy, we show that formation of the 12mer DegP cage accompanying hTRF1 binding is strongly cooperative. NMR studies of the structural dynamics of hTRF1 clients within the cages reveal that they adopt a predominantly unfolded ensemble with only subtle interactions with the long LA loops of DegP that project into the cage interior. DegP proteolysis assays of hTRF1 show little influence of the LA loops on cleavage activity, however, dynamic light scattering (DLS) measurements of DegP assembly reveal that these long, unfolded elements play a key role in regulating higher-order oligomerization by controlling the concentration of M_{6A} and hence the relative importance of paths A and B (Figure 1A). Finally, the interplay between substrate binding and interprotomer allosteric communication was investigated via peptidase assays involving molecules containing mixtures of WT and mutant protomers, through which a cooperative structural transition was uncovered at the level of the protease domains of DegP that gives rise to efficient proteolysis. Taken together, our biophysical study of DegP:client interactions establishes a

https://doi.org/10.1021/jacs.3c13247
J. Am. Chem. Soc. 2024, 146, 8242−8259

highly dynamic and cooperative molecular machine that is primed for regulating periplasmic protein homeostasis.

2. MATERIALS AND METHODS

2.1. Plasmid Constructs and Cloning. The expression constructs corresponding to *E. coli* DegP (strain K12) and human hTRF1 were as described in previous studies;[18,31] expression generated N-terminally His_6-SUMO tagged proteins for affinity purification. Mutant constructs of DegP and hTRF1 were generated using Phusion DNA polymerase and the Quikchange site-directed mutagenesis method.

2.2. Protein Expression. DegP and hTRF1 were expressed as described earlier.[18,31] For producing [U-^{2}H, Ileδ1-$^{13}CH_3$, Leu/Val-$^{13}CH_3$/$^{12}CD_3$, Metε-$^{13}CH_3$]-labeled proteins (referred to as ILVM labeling in the text; isopropyl methyl groups are not stereospecifically labeled) transformed cells were grown in minimal M9 D_2O media supplemented with d_7-glucose as the sole carbon source along with the addition of 60 mg/L 2-keto-3-d_2-4-^{13}C-butyrate for Ileδ1, 80 mg/L 2-keto-3-methyl-d_3-3-d_1-4-^{13}C-butyrate for Leu,Val-$^{13}CH_3$/$^{12}CD_3$,[35] and 100 mg/L methyl-$^{13}CH_3$-methionine for Metε.[36] For the production of [U-^{2}H, Ileδ1-$^{13}CH_3$, Leuδ1-$^{13}CH_3$, Valγ1-$^{13}CH_3$, Metε-$^{13}CH_3$]-hTRF1 (for stereospecific assignments of isopropyl methyl groups of the DegP-bound client), 230 mg/L 2-hydroxy-2-methyl-d_3-3-oxobutanoate-4-^{13}C was added, generating Leuδ1,Valγ1-$^{13}CH_3$, and proR methyl labeling.[37] Precursors were added 1 h before induction of protein overexpression. Uniformly deuterated proteins (denoted as U-^{2}H) were also grown in D_2O M9 minimal media except that protein expression was induced without addition of the precursors for methyl labeling.

2.3. Protein Purification. Briefly, after expression at 25 °C for ∼16−20 h, the cell pellets were collected via centrifugation, resuspended in buffer containing 6 M Gdn HCl, and lysed. The cleared lysates obtained after centrifugation were then applied to nickel affinity purification columns. This step was also performed with buffer containing 6 M Gdn HCl to wash away bound clients in the case of DegP and to prevent proteolysis of hTRF1 by cellular proteases. hTRF1 was refolded on the column with a 6 to 0 M Gdn HCl single step wash prior to elution. DegP was eluted in Gdn HCl buffer and refolded by rapid dilution into buffer without Gdn HCl. The His_6-SUMO tags were subsequently cleaved using Ulp1 protease, followed by either a cation exchange (hTRF1) or a hydrophobic chromatography step (DegP). Fractions corresponding to the hTRF1 or DegP peaks were pooled and then subjected to gel filtration as a final purification step. In all cases, purified proteins were buffer exchanged into final buffers used for experiments (given in each section subsequently) via Amicon Ultra-15 concentrators. The concentrations of purified samples were measured using a NanoDrop spectrophotometer, and their extinction coefficients at 280 nm were obtained from an online calculator (7575 and 24,980 M^{-1} cm^{-1} for DegP and hTRF1 respectively; https://web.expasy.org/protparam).

2.4. Sedimentation Velocity AUC Experiments (Figure 1C,D). AUC data for S210A DegP as a function of increasing molar equivalents of hTRF1 were collected in a buffer consisting of 25 mM HEPES free acid, 25 mM NaCl, 1 mM EDTA, pH 7.0, at 20 °C. Sedimentation velocity (SV) AUC experiments were performed using a ProteomeLab XL-I ultracentrifuge (Beckman Coulter, Indianapolis, IN) following protocols described previously[38,39] with minor modifications. Briefly, 400 μL samples were loaded into AUC cell assemblies with 3 or 12 mm charcoal-filled Epon double-sector centerpieces. After inserting cells into an An-50TI rotor and mounting in the centrifuge chamber, the temperature was equilibrated for ∼3 h, followed by acceleration to 30,000 or 45,000 rpm. Sedimentation profiles for each sample were acquired using both absorbance (280 nm) and interference optical detection systems.

SV analysis was carried out with SEDFIT (V16p34b) using the standard c(s) model which does not account for the nonideality of sedimentation and diffusion;[40] these effects are typically small below ∼200 μM total monomer concentration, M_T (∼9.4 mg mL^{-1}). Sedimentation coefficient distributions were normalized to water at 20 °C using SEDNTERP,[41] exported from GUSSI,[42] and visualized using an in-house Python script.

2.5. NMR Measurements (Figures 2 and 3). NMR experiments were recorded on Bruker Avance III HD 14.1 or 18.8 T spectrometers equipped with cryogenically cooled, pulsed-field *X,Y,Z*-gradient, triple-resonance probes. All NMR spectra were processed using NMRPipe[43] and visualized using NMRFAM-SPARKY,[44] CCPNMR Analysis,[45] and nmrglue.[46] Peak fitting for quantifying ΔR_2 and $S^2\tau_c$ values was performed using peakipy (https://j-brady.github.io/peakipy/). In what follows, each NMR experiment was measured in 25 mM HEPES free acid, 25 mM NaCl, 1 mM EDTA, 99.9% D_2O, pH 7.0 (pD 7.4).

Assignments of methyl side chains of the PDZ1 domain of ILVM-labeled S210A DegP were transferred from those obtained for the isolated PDZ1 domain using standard triple resonance methods.[47] Methyl resonance assignments of ILVM-labeled hTRF1 within the U-^{2}H S210A DegP 12mer were obtained via preparation of a series of ILVM-labeled hTRF1 mutants where the methyl-bearing side chains were sequentially mutated to Ile (except for I30 as it is the only Ile residue). Complexes were then formed with U-^{2}H S210A DegP, and HMQC spectra were measured at 40 °C and 14.1 T. The assignments were readily obtained through a comparison of these spectra with the HMQC spectrum of WT ILVM-labeled hTRF1 bound to U-^{2}H S210A DegP collected under the same conditions. Assignments were then easily transferred to the HMQC spectrum of ILVM-labeled hTRF1 encapsulated by U-^{2}H S210A Δloops DegP. Stereospecific assignments of the Leu and Val resonances in the bound ILVM-labeled hTRF1 spectrum were generated from a sample where only the Leuδ1 and Valγ1 methyl groups (proR) were isotopically labeled.

Spectra shown in Figures 2B and 3D were obtained as HMQC data sets (18.8 T) that exploit the methyl-TROSY effect.[48] These were recorded as a titration series of ILVM-labeled S210A DegP (100 μM) with U-^{2}H hTRF1 (0, 10, 20, 30, 50, 75, 100, 150, and 200 μM) at 50 °C (Figure 2B), or as single spectra of unbound ILVM-labeled hTRF1 (Figure 3D, left, 100 μM) or ILVM-labeled hTRF1 in complex with either U-^{2}H S210A DegP or S210A Δloops DegP at 40 °C (in these cases, 300 μM ILVM-labeled hTRF1 and 600 μM of the two different U-^{2}H DegP constructs were used; Figure 3D center and right).

Diffusion constants for ILVM-labeled hTRF1, both unbound and in complex with the U-^{2}H DegP constructs were extracted from the profiles as shown in Figure 3C that reflect the decay of the methyl peak intensities resulting from 1D HSQC-based pulsed-field gradient experiments measured using a pulse scheme similar to that published previously,[49] with ^{15}N and ^{13}C pulses interchanged. Data sets were recorded at 40 °C and 18.8 T and the initial experiments, performed in a 5 mm tube, were repeated in a 3 mm tube to test whether convective currents biased the measured diffusion constants; no differences were found. Additionally, diffusion constants were measured using different diffusion times to ensure the absence of convection and again differences were not observed.

2.6. Measurements of hTRF1 Dynamics Inside DegP Cages.

2.6.1. Methyl-TROSY Based CPMG Measurements (Figures 3E, S2 and S3). Methyl ^{1}H-^{13}C multiple quantum CPMG experiments were recorded at 40 °C and 18.8 T using the pulse scheme of Korzhnev and co-workers.[50] A constant-time relaxation delay, T_{relax}, of 12 ms was used, along with ν_{CPMG} frequencies varying from 83.3 to 2000 Hz, with two duplicate points to estimate errors. Effective transverse relaxation rates, $R_{2,eff}$, were calculated as $R_{2,eff} = -(1/T_{relax}) \ln (I/I_0)$, where I and I_0 are the intensities of peaks recorded in spectra with and without the T_{relax} delay, respectively. ΔR_2 values shown in Figures 3E and S3 were calculated as $R_{2,eff}$ (83.3 Hz) − $R_{2,eff}$ (2000 Hz) from the experimental profiles, examples of which are shown in Figure S2. Note that 83.3 Hz (2000 Hz) is the smallest (largest) frequency used in recording the CPMG data set.

2.6.2. Measuring Methyl $S^2\tau_c$ Values (Figure 3F). $S^2\tau_c$ values for ILVM-labeled hTRF1 in complex with either of the two U-^{2}H DegP constructs (Figure 3F) were measured as described previously, where sums (I_{SQ}) and differences (I_{3Q}) of single quantum methyl ^{1}H magnetization components are quantified.[51] This was achieved using 15 relaxation delays (1, 1.4, 1.8, 2.2, 2.6, 3, 3.5, 4, 4.5, 5, 6, 7, 8, 9, and

https://doi.org/10.1021/jacs.3c13247
J. Am. Chem. Soc. 2024, 146, 8242−8259

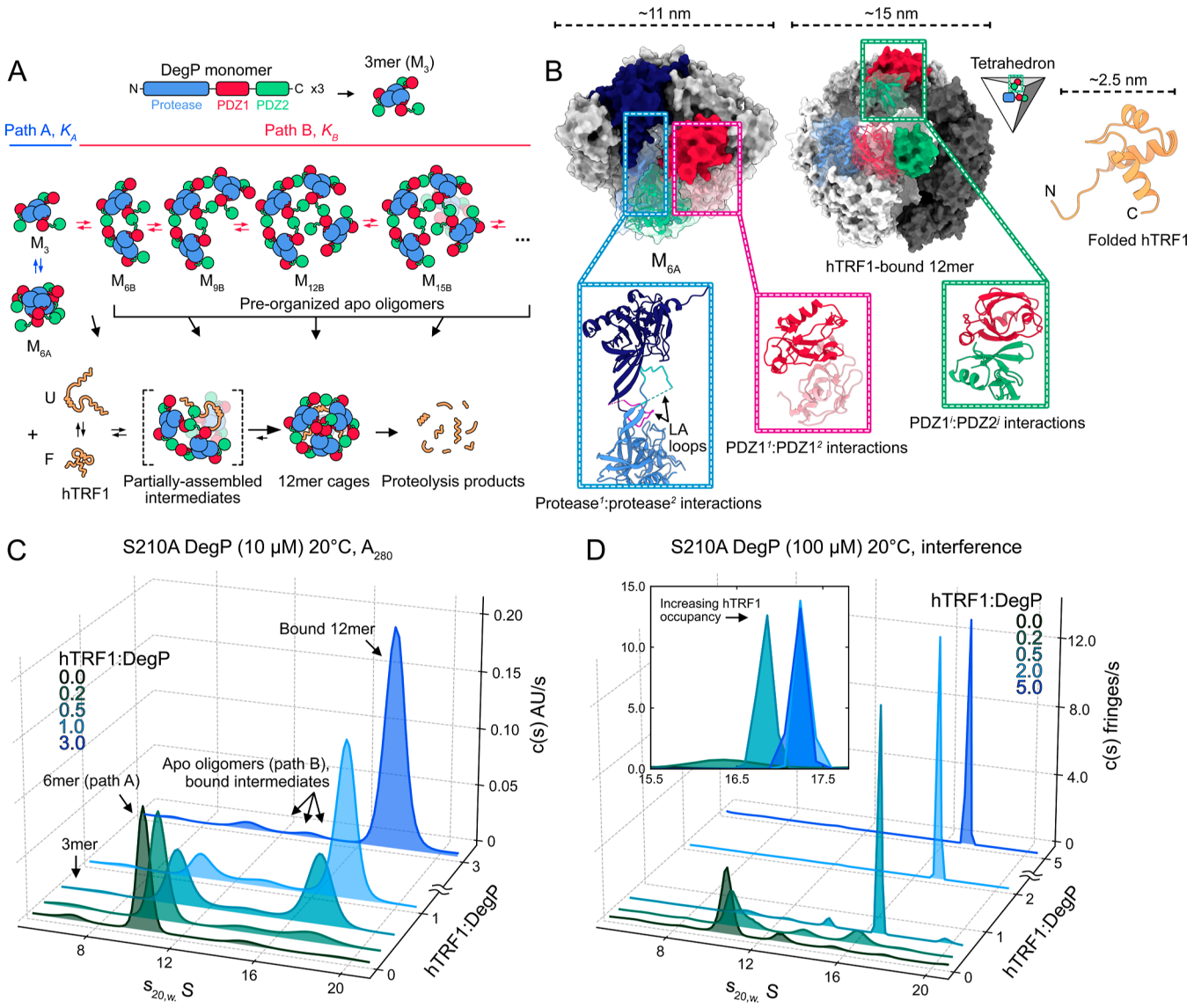

Figure 1. Client binding results in cooperative DegP cage formation as studied by AUC. (A) DegP monomer architecture (top) and oligomeric ensemble in the absence and presence of the model client protein hTRF1 (middle and bottom). (B) Structures of apo M_{6A} (left, PDB 1KY9) and the tetrahedral hTRF1-bound 12mer (middle, PDB 8F0U; a cartoon tetrahedron with intertrimer contacts for a single protomer from the white trimer is displayed to the upper right of the 12mer), along with the model client protein hTRF1 (right, PDB 1BA5). Intertrimer interaction interfaces are highlighted for M_{6A} and the 12mer. M_{6A} is stabilized by intertrimer protease^1:protease^2 and PDZ1^1:PDZ1^2 interactions; the superscripted integers denote domains from trimers 1 and 2. Protease and PDZ1 domains of the top and bottom trimers are highlighted in the magnified views with dark and light colors, respectively, to better visualize the domains involved in the oligomeric interface. The 12mer is formed via intertrimer PDZ1^i:PDZ2^j interactions [$i, j \in (1, 2, 3, 4)$ as there are four trimers in the complex, $i \neq j$]. In each of the M_{6A} and 12mer structures, domains from the same protomer of a trimer are shown in ribbon representation with transparent surfaces; domains interacting with these are shown in colored surface representation and derive from protomers in separate trimers. (C) Sedimentation coefficient distributions obtained from SV AUC experiments where the sample absorbance at 280 nm was monitored for mixtures of 10 μM (protomer concentration) S210A DegP and 0, 2, 5, 10, and 30 μM hTRF1 at 20 °C. (D) As (C), except obtained through interference optics measurements of samples consisting of 100 μM S210A DegP and 0, 20, 50, 200, and 500 μM hTRF1 at 20 °C. The inset depicts the shift of the bound 12mer peak to larger $s_{20,w}$ values as the cages are increasingly saturated with hTRF1.

10 ms) with 16 and 24 scans for measuring I_{SQ} and I_{3Q}, respectively. These experiments were recorded at 40 °C and 18.8 T and analyzed as described previously.[51]

2.6.3. Proteolysis Assays by SDS PAGE (Figures 4B,C and S4). Samples for SDS PAGE-based analyses of the kinetics of hTRF1 cleavage were prepared in 100 μL volumes containing 10 μM DegP or Δloops DegP and 100 μM hTRF1, or 30 μM DegP and 30 μM hTRF1. The experiments with a 1:10 DegP:hTRF1 molar ratio were incubated at 30 or 37 °C in a heating block for the duration of the reaction. For the experiments with a 1:1 molar ratio, reactions took place in a cold room at 4 °C. In all cases, time points were obtained through the removal of 10 μL aliquots from the main reaction volume, to which 10 μL of gel loading buffer containing SDS was added to denature DegP and quench the reaction. For a $t = 0$ point, a separate sample of 100 μM hTRF1 was prepared from which an aliquot was extracted and mixed with SDS loading buffer as above. The gels were loaded with a 5 μL volume of the quenched reaction aliquots in the 1:10 molar ratio experiments (Figure 4B) and 15 μL in the 1:1 case (Figure S4A). The increased loading volume for the 1:1 molar ratio experiment was necessary in order to visualize the hTRF1 band given the lower initial concentration as compared to the 1:10 reaction. The proteins therein were resolved on the gels by application of 200 V for

https://doi.org/10.1021/jacs.3c13247
J. Am. Chem. Soc. 2024, 146, 8242−8259

25 min. To reveal the bands corresponding to DegP and the hTRF1 cleavage products, the gels were stained with Coomassie blue and then imaged with a BioRad Gel Doc imaging system. Decay profiles for the reactions, as shown in Figures 4C and S4B, were generated by integrating the intact hTRF1 bands using ImageJ[52] followed by normalization against the $t = 0$ hTRF1 band intensity measured in the absence of DegP. Profiles were fit with exponential functions to obtain effective decay rate constants (k) for the hTRF1 cleavage reactions at each temperature.

2.6.4. DLS Measurements and Autocorrelation Analysis (Figures 5B and S5). DLS autocorrelation functions for generating DLS data sets were recorded using a plate reader format Wyatt DynaPro DLS instrument with a 150° detector angle and 824 nm laser irradiation. For the DLS data sets shown in Figure 5B, protein samples were prepared in 25 mM NaH_2PO_4, 200 mM NaCl, 1 mM EDTA, pH 7.0, while those in Figure S5 were measured with samples in buffer containing 25 mM HEPES free acid, 25 mM NaCl, 1 mM EDTA, pH 7.0. Samples for DLS measurements were prepared as described previously.[18,31] Autocorrelation functions for each sample well in the plate reader format instrument were measured over the temperature range 5−50 °C in discrete increments of 2.5 °C for a total sampling of 19 temperature points. Each well was measured 25 times per temperature with an acquisition time of 1 s per measurement. A final autocorrelation function for each well at a given temperature was obtained by averaging of the 25 replicates. In cases where an autocorrelation replicate was found to be artifactual due to dust or a bubble (characterized by a noisy baseline or an anomalously slow decay), the replicate was manually filtered from the data set. D_z values were extracted from the average autocorrelation functions using an in-house Python script applying the cumulants method.[53,54]

2.6.5. Preparation of Mixed Proteins (Figures 6D,E and S6). Mixed protein samples for peptidase activity measurements were prepared by combining WT and S183A DegP or F289A/Y444A and S183A/F289A/Y444A DegP (the F289A/Y444A mutations abrogate higher-order oligomerization, i.e., this construct can only form trimers; Figure S5) in a buffer of 25 mM NaH_2PO_4, 200 mM NaCl, 1 mM EDTA, pH 7.0 in various molar ratios to obtain total monomer concentrations of 500 μM in 80 μL volumes. Subsequently, 720 μL of the above buffer containing 6 M Gdn HCl was added to each mixed sample to denature the monomers therein. These were then rapidly diluted into 15 mL of the buffer without Gdn HCl (~20-fold dilution) to refold the monomers and generate mixed trimers. Samples that were 100% of a single protomer type (for example, all WT or all S183A) were also prepared according to this method. Aliquots of "100%" samples were subjected to gel filtration to test for the presence of aggregates arising from the refolding procedure; aggregation was not observed. The mixed samples were then buffer exchanged into assay buffer consisting of 25 mM HEPES free acid, 25 mM NaCl, 1 mM EDTA, pH 7.0 and concentrated to total monomer concentrations of approximately 200 μM in 200 μL volumes. Sample concentrations were verified using the extinction coefficients at 280 nm for WT or F289A/Y444A DegP (7575 and 6085 M^{-1} cm^{-1} respectively; the S183A mutation in either background does not change these values and therefore it is not necessary to take into account differences in the extinction coefficients between, e.g., WT and S183A DegP protomers).

2.6.6. Peptidase Assays with Mixed DegP Samples (Figures 6E and S6C). Mixed DegP samples for peptidase assays were prepared at 12.5 μM total monomer concentration with 2.5 mM of an activator peptide corresponding to the C-terminal 10 residues of hTRF1 (N-···KDRWRTMKKL-C in the full-length protein) that binds to the PDZ1 domains to promote a proteolytically active DegP conformation and induces cage formation (assembly into cages does not occur for the F289A/Y444A mutant, Figure S5). Aliquots (40 μL) of these stocks were then pipetted into the wells of a black polystyrene plate which was subsequently incubated within a Synergy Neo II plate reader for 5 min at 25 °C to equilibrate the sample temperature. To initiate the peptidase reaction, 10 μL of 1 mM fluorescently labeled substrate peptide was added which binds to the protease domains of DegP and is subsequently cleaved, leading to an increase in fluorescence (Abz-KASPV|SLG(Y-3NO_2)D; Abz denotes an amino-benzoic acid group, the vertical bar indicates the cleavage site, and (Y-3NO_2) is 3-nitrotyrosine).[29] After addition of all reactants, the final reaction concentrations were 10 μM DegP, 2 mM activator peptide, and 200 μM of substrate peptide in 50 μL. All reactions were performed in a buffer of 25 mM HEPES free acid, 25 mM NaCl, 1 mM EDTA, pH 7.0 (note that all protein and peptide stocks were also prepared in and diluted with this buffer). The reaction progress was monitored at 25 °C through the increase in fluorescence at 420 nm using an excitation wavelength of 320 nm. Cleavage rates were obtained from the initial, linear regions of the activity curves and normalized to the maximum rate obtained with 100% of either WT or F289A/Y444A protomers, yielding the profiles, as shown in Figure 6E. Reactions were performed in triplicate to estimate errors in the rates.

3. RESULTS

3.1. hTRF1 Induces Cooperative Assembly of DegP Cages with Few Intermediates. As a first step toward understanding the mechanism of cage assembly in response to hTRF1 engagement, we performed SV AUC experiments monitoring the size distribution of S210A DegP cage particles as a function of the addition of client. Here, we have used a construct lacking the catalytic serine (S210) to prevent autocleavage. Figure 1C,D shows calculated sedimentation coefficient (corrected to 20 °C in water, $s_{20,w}$) distributions [c(s)] obtained from modeling of the experimental profiles recorded using protomer concentrations of 10 and 100 μM, respectively. These concentrations were selected to explore hTRF1-bound cage assembly over the biological range of DegP in the periplasm.[18] Note that in Figure 1C, the c(s) distributions were derived from experiments that measured the sample absorbance at 280 nm to define the shape of the sedimentation boundaries, while those in Figure 1D were extracted from data sets collected using interference optics due to the much higher sample concentrations used that cannot be accurately quantified by absorbance measurements. Analysis and comparison of peak shapes are complicated by the numerical deconvolution procedure applied to the data[55] so that peak widths, for example, cannot be used to evaluate the distribution of species over a given $s_{20,w}$ value; peak integrals, however, provide robust measures of the relative populations of the sedimenting particles. In the absence of client and at either S210A DegP concentration (dark green traces), most of the signal in the distributions corresponded to a roughly 11S species which we had previously assigned to M_{6A}.[18] We also observed signatures for the 3mer (~6S) and higher-order path B assemblies (~13S−15S), albeit in much less amounts in comparison to M_{6A}. In keeping with higher protomer concentrations driving the assembly of path B oligomers via addition of trimers, somewhat elevated signal was observed in the ~13S−15S region at 100 μM S210A DegP (Figure 1D, dark green) with a reduction of the free 3mer and M_{6A} signal in the profile as compared to the 10 μM S210A DegP case (Figure 1C, dark green). The abundance of M_{6A} in each profile is consistent with its relative stability under these solution conditions (20 °C and 25 mM NaCl), as established previously.[18]

Addition of increasing molar equivalents of hTRF1 resulted in the buildup of a dominant ~17S species, consistent with an hTRF1-bound 12mer cage structure (Figure 1C,D, dark blue curves), which is the predominant species formed through interactions with this client.[18,31] The exact position of the 12mer varies between the two S210A DegP profiles (10 μM vs

https://doi.org/10.1021/jacs.3c13247
J. Am. Chem. Soc. 2024, 146, 8242−8259

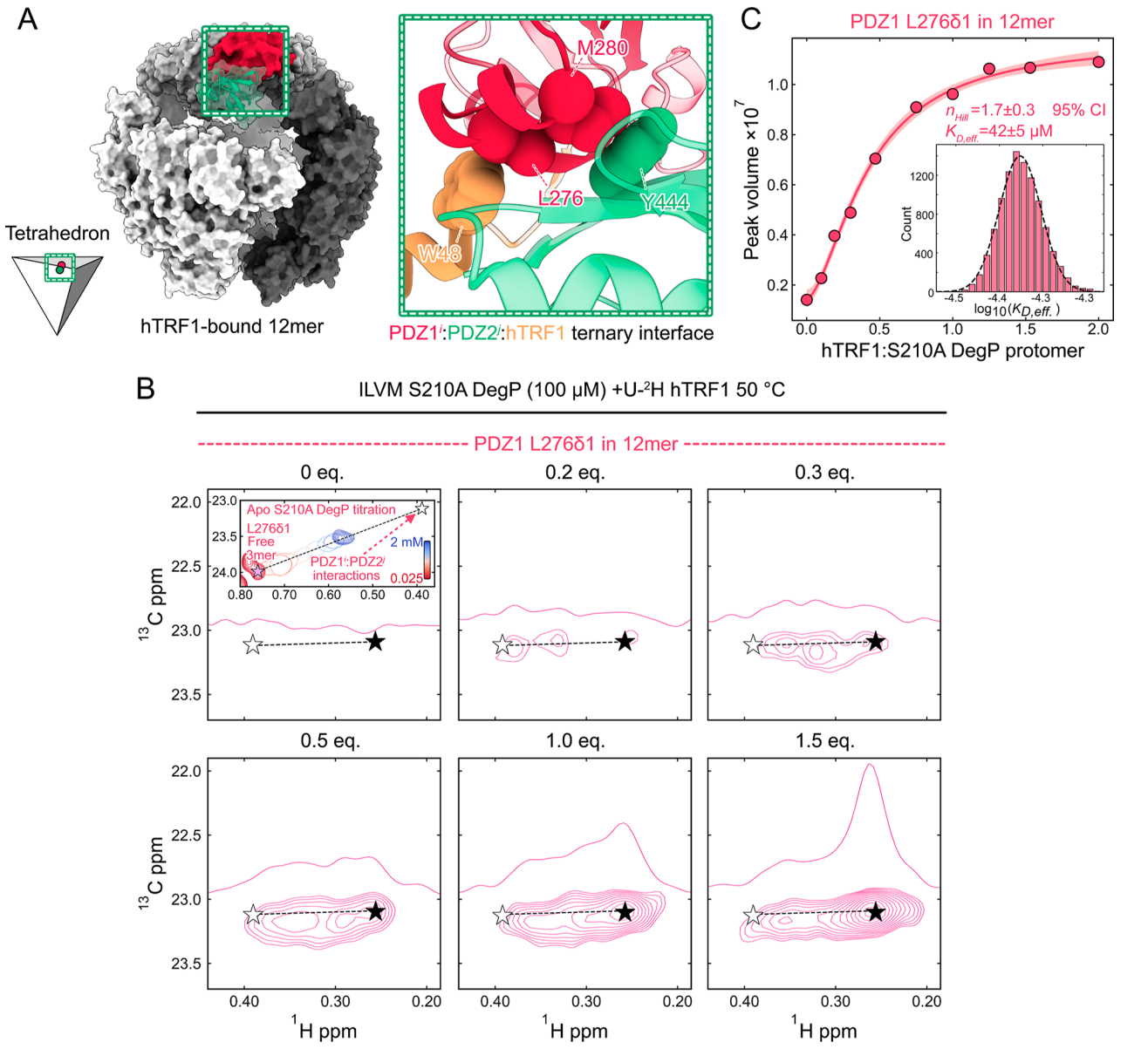

Figure 2. Monitoring substrate binding and DegP cage formation via methyl-TROSY NMR. (A) Structure of the tetrahedral hTRF1-bound DegP 12mer (PDB 8F0U), highlighting a PDZ1^i:PDZ2^j interaction between the light gray and white trimers, as illustrated schematically by the cartoon tetrahedron shown to the bottom left of the 12mer cage. Key residues involved in the ternary hTRF1:PDZ1^i:PDZ2^j interfaces that stabilize the complex are shown in the magnified view to the right with W48 in orange derived from hTRF1. (B) ^{13}C-^{1}H HMQC spectra of 100 μM ILVM-labeled S210A DegP with 0, 20, 30, 50, 100, and 150 μM U-^{2}H hTRF1 at 50 °C highlighting the region containing the PDZ1 L276δ1 methyl crosspeak in the 12mer over the course of the titration. White and black stars denote peak positions of L276δ1 in trimers of a 12mer cage where all three PDZ1 domains of a trimer are either unbound or fully bound with hTRF1, respectively. A trace through the center of the peaks is illustrated in each panel. The inset shows a superposition of ^{13}C-^{1}H HMQC spectra recorded for a concentration series of apo ILVM S210A DegP (0.025−2 mM protomer concentration, dark red to dark blue contours).[18] The pink star highlights the L276δ1 chemical shift obtained from a trimer mutant of DegP, i.e., the limit where no intertrimer interactions are present, and the white star is placed at the chemical shift position of the L276δ1 methyl group in the context of the 12mer cage where all PDZ1^i:PDZ2^j contacts are adopted (same white star is shown in each of the main panels). Some of the peaks within the vicinity of L276δ1 in the inset have not been displayed for clarity. As a function of protomer concentration, S210A DegP forms an ensemble of rapidly exchanging oligomers that do not feature the full complement of PDZ domain interactions[18] and therefore the L276δ1 resonance does not reach the white star (inset). Binding of substrate is necessary to shift the apo ensemble to 12mers, at which point a correlation for the L276δ1 methyl initially appears at the position of the white star, with additional peaks extending to the black star forming with higher concentrations of hTRF1 (main panels). (C) Binding isotherm generated from the titration in (B) for the L276δ1 methyl group and fit to a modified Hill equation (red curve) according to $V = \Delta V \frac{[\text{hTRF1}]^{n\text{Hill}}}{K_{\text{D,eff}}{}^{n\text{Hill}} + [\text{hTRF1}]^{n\text{Hill}}} + a$, where V is the peak volume, ΔV and a are scaling and offset parameters estimated from the minimum and maximum values of the isotherm, respectively, and $K_{\text{D,eff}}$ and n_{Hill} are the effective dissociation constant and Hill cooperativity parameter, respectively. The optimal values for $K_{\text{D,eff}}$ and n_{Hill} obtained from the fit are 42 ± 5 μM and 1.7 ± 0.3 respectively. The shaded region encompassing the best-fit curve corresponds to the 95% confidence interval. The inset shows the associated distribution of $K_{\text{D,eff}}$ values obtained via Monte Carlo simulations.[81]

https://doi.org/10.1021/jacs.3c13247
J. Am. Chem. Soc. 2024, 146, 8242−8259

100 μM) due to solution nonideality effects that occur at the higher protein concentrations employed.[56−58] Strikingly, the appearance of the ∼17S species occurred with substoichiometric quantities of hTRF1 at either concentration of S210A DegP, suggesting that 12mer cage formation does not require saturation of trimers with client chains. This is best exemplified by the titration of 100 μM S210A DegP with hTRF1 (Figure 1D) where near complete formation of the 12mer cage is achieved with the addition of 0.5 equiv of client (0.5 hTRF1:1 protomer of DegP). Further to this point, the inset to Figure 1D highlights the shift of the 12mer peak as a function of hTRF1 (from ∼16.4S to ∼17.3S), indicating that the initially formed cages are only partially ligated. Concomitant with the buildup of the 12mer species, the signal for M_{6A} decreased. In addition, signals within the 13S−15S region were also diminished, establishing that the concentration of apo-intermediate oligomers was reduced, without formation of partly assembled hTRF1-bound intermediates. Notably, the buildup of the 12mer cage was much more gradual for the lower S210A DegP concentration, as would be expected.

The absence of appreciable amounts of intermediate species in the formation of the 12mer is one of the hallmarks of cooperative, all-or-nothing self-assembly,[59,60] as observed for many other protein assemblies including virus capsids[60] and engineered protein cages,[59] where only free subunits and the fully assembled architecture are present at equilibrium, with their relative amounts governed by the total protein concentration. To obtain a quantitative measure of cooperativity in the assembly of the 12mer cage, driven by the binding of hTRF1, we generated weighted *s*-value (s_w) isotherms by integrating over the regions of the c(s) distributions that includes all DegP particles, from trimer to 12mer (Figure S1). An inspection of these curves revealed sigmoidal behavior, consistent with a positively cooperative transition (i.e., interactions that increase in strength as the assembly proceeds). We modeled the sigmoidal isotherms using the Hill equation (Figure S1A,B, left), which provides an effective measure of cooperative interactions and obtained best-fit Hill coefficients of 1.6 ± 0.2 and 2.4 ± 0.2 for the 10 and 100 μM S210A DegP titrations, respectively, in further support of the cooperative nature of 12mer assembly, along with values of the effective dissociation constants, $K_{D,eff}$, of 4.9 ± 0.3 (10 μM S210A DegP) and 33 ± 2 μM (100 μM S210A DegP). We note that the interpretation of $K_{D,eff}$ is, however, complicated by the fact that a number of processes contribute to cage formation, including the actual client binding event, dissolution of preorganized apo oligomers (the distribution and populations of which depend on the total protomer concentration, though M_{6A} is the dominant species at 20 °C where our AUC experiments were performed),[18] and assembly of highly populated 12mer structures upon client binding. We additionally performed fits of the data where we fixed the Hill coefficient to 1 to assess whether our binding data could be modeled as a noncooperative transition. Poor fits of the isotherms were obtained in this case (Figure S1A,B, right). It is important to emphasize that the Hill model, while inherently simple, is only useful in providing a qualitative framework to visualize the cooperativity, with little insight obtained regarding the details of the hTRF1 binding and cage formation process.

Having established by AUC that 12mer cage formation is cooperative, we next asked whether additional insights into the assembly process could be obtained by solution NMR spectroscopy. Considering that the formation of PDZ1^i:PDZ2^j interactions serve as the structural hallmark for the adoption of cages,[28] we examined the intertrimer interfaces in the 12mer structure for residues that could be direct reporters of client binding and cage assembly using solution NMR. Figure 2A illustrates the hTRF1-bound 12mer structure,[31] highlighting a PDZ1^i:PDZ2^j interaction that displays an intimate arrangement of aromatic side chains from hTRF1 (W48) and PDZ2^j (Y444) that are juxtaposed against L276 of PDZ1^i, among other residues (e.g., M280). As we had previously shown that the interaction of isolated PDZ1 and PDZ2 domains from DegP is accompanied by substantial chemical shift changes for some of the PDZ1 methyl groups, we focused on these for further NMR studies in the presence of hTRF1. Owing to the large size of the DegP:hTRF1 complexes formed (∼600 kDa), we prepared highly deuterated protein, with $^{13}CH_3$ labeling at Ile-δ, Leu-δ, Val-γ, and Met-ε positions, where only one of the pair of isopropyl methyls of Leu and Val was $^{13}CH_3$ labeled (referred to as ILVM-labeling in what follows) and recorded ^{13}C-^{1}H heteronuclear multiple quantum coherence (HMQC) spectra that exploit the methyl-TROSY principle.[48,61] A series of spectral regions focusing on L276δ1 from spectra of ILVM-labeled S210A DegP recorded during a titration with uniformly deuterated (hereafter denoted U-^{2}H) hTRF1, and extending from 0 to 1.5 equiv of the client (per DegP protomer), is shown in Figure 2B. The inset in the first panel of this figure shows a concentration series for apo S210A DegP (from 0.025 to 2 mM protomer concentration) that we have published previously[18] and is reproduced here for illustrative purposes. In the absence of client, and at low S210A DegP concentrations, the L276δ1 chemical shift appears near the free trimer position, highlighted by the pink star, and proceeds along the trajectory depicted by the black dashed line as the labile ensemble of partly assembled apo species is populated. Since members of the ensemble cannot form the full complement of PDZ1^i:PDZ2^j interactions without addition of client to drive cage formation,[18] the L276δ1 resonance does not reach the end point of this trajectory indicated by the white star, which marks the frequency where all possible PDZ1^i:PDZ2^j contacts are adopted, as in discrete, substrate-bound cages. We obtained this end point from a separate titration involving isolated PDZ1 and PDZ2 domains, which served as a proxy for cage assembly.[18] As a function of increasing hTRF1 concentration, however, a series of peaks emerge, with an initial peak at the position of the white star at low concentrations of hTRF1, corresponding to a fully formed 12mer. As the concentration of hTRF1 is increased, the number of peaks grows (Figure 2B), likely reflecting the partial occupancy of the DegP binding sites and the fact that the L276δ1 chemical shift is sensitive to both the number and the position of bound hTRF1 ligands within each trimer unit. We attribute the most upfield peak, marked by the black star, to that of a fully bound trimer within the context of the 12mer cage as its intensity increases as a function of increasing hTRF1 concentration. Notably, at 1.5 equiv, there are still multiple peaks, suggesting that full binding at all 12 sites of the 12mer does not occur under these conditions, with the small population at the position of the white star likely reflecting trimers within 12mer structures that are not saturated with hTRF1, and not completely unbound cages. Similar to our AUC measurements, the isotherm obtained from the titration exhibited sigmoidal character, consistent with positively cooperative binding and assembly. The isotherm was fit to the Hill equation, yielding a best-fit

https://doi.org/10.1021/jacs.3c13247
J. Am. Chem. Soc. 2024, 146, 8242−8259

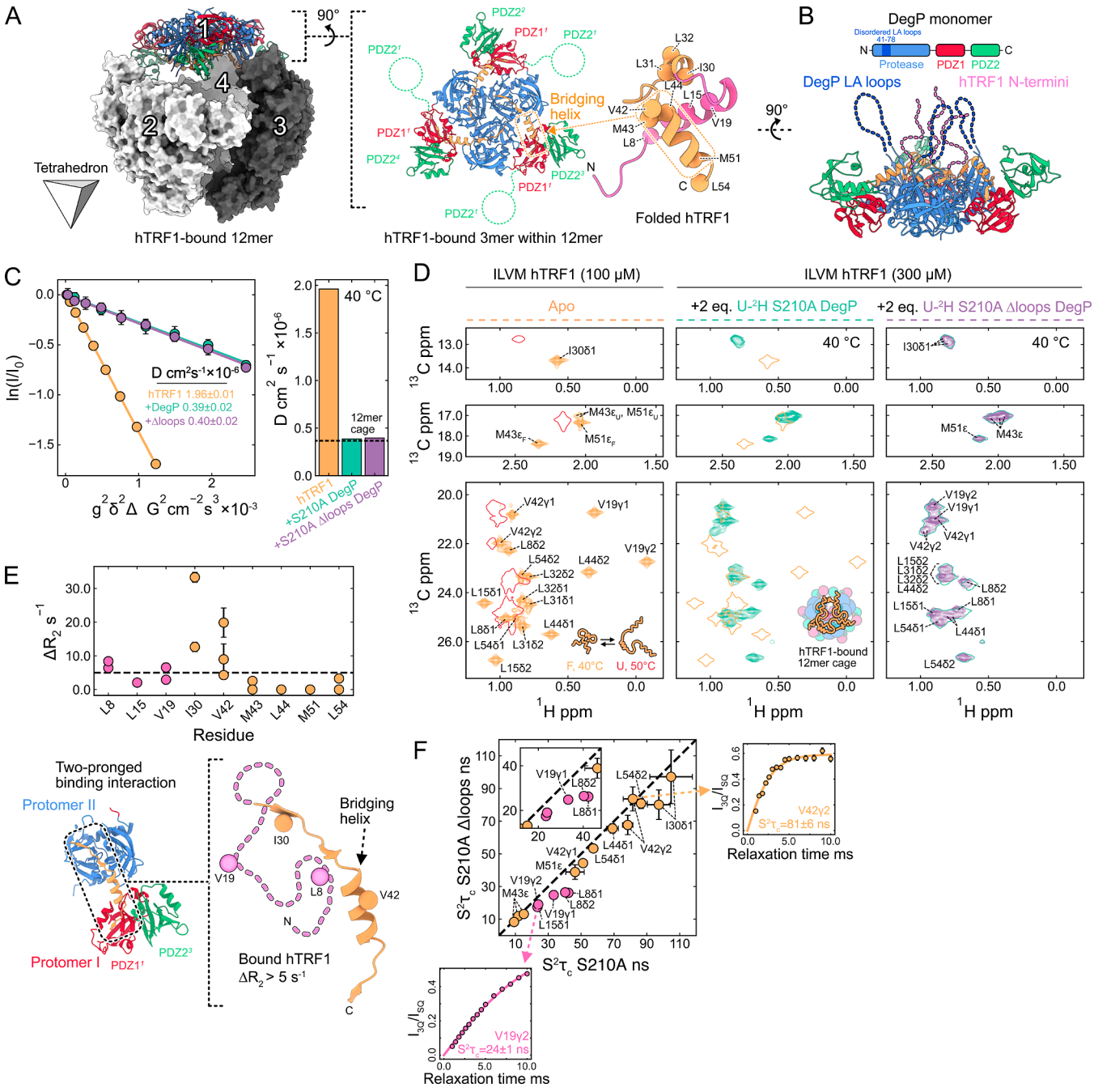

Figure 3. Probing structural dynamics of client hTRF1 bound to the DegP 12mer cage by methyl-TROSY NMR. (A) Cryo-EM structure of a tetrahedral hTRF1-bound 12mer cage with the top trimer (trimer 1 of 4) shown in colored ribbon representation (left, PDB 8F0U; a cartoon tetrahedron is shown at the bottom left in the same orientation for comparison) and rotated by 90° to reveal the inner face where the C-terminal region of hTRF1 is engaged (middle, the C-terminal portion of the hTRF1 chain is shown in orange). Note that the C-terminal half of hTRF1 is bound by the PDZ1 domain of one protomer and the protease domain of a counterclockwise related adjacent protomer; a natively folded helix bridges the two binding sites. The superscripted integers in the PDZ domain labels denote the trimer from which the domains originate (A, left). The PDZ2 domains from the displayed trimer (trimer 1; 3 $PDZ2^1$ domains) form interactions with other trimers within the 12mer and are not visible in this view (depicted with dashed green lines and circles). The folded, unbound structure of hTRF1 (PDB 1BA5) is shown to the right colored according to the N- and C-terminal halves. Methyl-bearing residues throughout the hTRF1 chain are indicated and shown as colored balls. (B) Side view of the DegP trimer from (A, middle) with the long, disordered LA loops of the protease domains and the N-termini of bound hTRF1 chains, both of which project into the interior of the cages and are not observed in the 12mer structure, drawn as dark blue and pink dashed curves, respectively. The DegP monomer architecture is shown above with the indicated residues corresponding to the section of the LA loops studied herein. (C) Intensity decay profiles for ILVM-labeled hTRF1 free (orange) or in complex with either U-^{2}H S210A (green) or U-^{2}H S210A Δloops (purple) DegP measured using 1D HSQC-based pulsed field gradient NMR experiments (left) at 40 °C from which diffusion constants were obtained from the slopes of the lines (equal to $-\gamma^2 D$) (right). The horizontal dashed black line (right) is the diffusion constant at infinite dilution for the 12mer cage, $D_{12,0}$, calculated according to a scaling law for spherical particles relating the diffusion constant of the 12mer to the number of 3mers, i.e., $D_{12,0} = D_{3,0} \times 4^{-1/3}$, where $D_{3,0}$ is the diffusion constant for the 3mer, 4 is the number of 3mers in the 12mer, and the −1/3 exponent accounts for the assumed spherical particle shape. The diffusion constant for the 3mer was calculated from the experimentally determined

https://doi.org/10.1021/jacs.3c13247
J. Am. Chem. Soc. 2024, 146, 8242−8259

Figure 3. continued

hydrodynamic radius (r_h) of 4.9 nm[18,31] using the Stokes−Einstein equation and the solution viscosity adjusted for temperature and the D_2O content of the sample buffer (99.9%). (D) ^{13}C-^{1}H HMQC spectra of 100 μM ILVM-labeled hTRF1 collected at 40 and 50 °C (left, orange and red, respectively), and 300 μM ILVM-labeled hTRF1 in the presence of either 600 μM U-^{2}H S210A DegP (middle, the single contour in orange corresponds to the 40 °C hTRF1 spectrum from the left panel) or 600 μM U-^{2}H S210A Δloops DegP (right, the single contour corresponds to the green spectrum from the middle panel), both of which were measured at 40 °C. (E) ΔR_2 values for methyl groups within ILVM-labeled hTRF1 bound to U-^{2}H S210A DegP (top), quantified as the difference between the effective transverse relaxation rates extracted from CPMG experiments with refocusing pulse trains of 83.3 and 2000 Hz. ΔR_2 values >5 s^{-1} are shown as colored balls on an hTRF1 chain (bottom) within the trimer from (A, middle). (F) Linear correlation plot of $S^2\tau_c$ values for methyl groups of hTRF1 bound to U-^{2}H S210A DegP (x-axis) or U-^{2}H S210A Δloops DegP (y-axis), 40 °C. The circles are colored according to the position of each methyl-bearing residue in the hTRF1 chain, as in (A, right). The dashed line is $y = x$, and the inset highlights the deviation of the N-terminal residues from the line. Ratios of differences (I_{3Q}) and sums (I_{SQ}) of single quantum methyl ^{1}H magnetization components (colored points) as a function of relaxation time for select methyl groups within the hTRF1 chain are shown to the right and bottom of the correlation plot. The $S^2\tau_c$ values extracted from fitting of the profiles (colored curves) are indicated.

value for the Hill coefficient of 1.7 ± 0.3 and $K_{D,eff}$ = 42 ± 5 μM (Figure 2C, the shaded region surrounding the fitted curve corresponds to the 95% confidence interval with associated distribution of $K_{D,eff}$ values shown in the inset), consistent with what we obtained from our AUC analyses.

3.2. hTRF1 is Largely Unfolded But Adopts Multiple Bound Conformations Inside 12mer Cages. NMR spectroscopy is a powerful tool for studies of the structural dynamics of intrinsically disordered regions (IDR) of proteins that, in general, are unobserved using other structural modalities. We have explored such dynamics in the context of hTRF1 within 12mer cage complexes, motivated, in part, by our previous cryo-EM studies of DegP cages in which we were unable to observe considerable portions of folded clients within these assemblies or the LA loops of the protease domains that may interact with substrates in the cage centers.[31] Prior to describing our NMR studies, we first provide, as background, a brief description of the structural information that is available for hTRF1 from our cryo-EM model of the 12mer complex. Focusing on trimer 1 of the hTRF1-bound 12mer in Figure 3A (left, ribbon) and, in particular, on the inner face of this trimer (Figure 3A, middle), it can be seen that each C-terminal half of an hTRF1 chain (orange) is engaged at its C-terminus by the PDZ1 domain of a protomer and in the active site within the protease domain of an adjacent protomer, related to the first in a counterclockwise manner. This bipartite binding mode is facilitated by residual native α-helical structure of the hTRF1 chain that bridges the two sites (Figure 3A middle and right). The N-terminal half, which also includes α-helical structure in the folded, unbound state (Figure 3A right, see the pink portion of the folded hTRF1 structure), projects toward the middle of the cage to potentially form interactions with the long, disordered LA loops of the protease domains (Figure 3B).

To address whether there are interactions between client and LA loops, a series of methyl TROSY-based experiments focused on ILVM-labeled hTRF1 in complex with either U-^{2}H S210A DegP or U-^{2}H S210A Δloops DegP were performed (the Δloops construct lacks residues 41−78 corresponding to the majority of each LA loop). The presence of methyl-bearing side chains throughout hTRF1 (a total of 11 ILVM residues) enabled us to probe the structural dynamics of both the N- and C-terminal halves (Figure 3A right, colored balls) of the client, while comparative studies of both S210A DegP and S210A Δloops DegP allowed for an assessment of potential differences in clients bound to cages either with or without the LA loops. To confirm that 12mer complexes were formed under the conditions of our NMR measurements, we first measured translational diffusion constants using pulsed-field gradient experiments[62] (Figure 3C left). The diffusion constant for hTRF1 in either DegP complex was ∼4.8-fold smaller than for unbound hTRF1 (Figure 3C right), consistent with an increase in molecular mass of ∼100-fold (as would be the case for spherical particles; M_{hTRF1} = 6.7 kDa for reference). In addition, diffusion values were in excellent agreement with those predicted for a 12mer cage (Figure 3C right, black dashed line).

Given the high molecular weight of the DegP 12mer complex, we were interested in recording spectra at a reasonably high temperature that would still support the folded hTRF1 structure present in the unbound state. With this in mind, we first collected a series of HMQC spectra for apo ILVM-labeled hTRF1 as a function of temperature (Figure 3D left). At 40 °C, the HMQC spectrum indicated that hTRF1 was folded (orange spectrum), as expected based on previous NMR studies at this temperature (although under different buffer conditions[63]), while increasing the temperature to 50 °C led to unfolding (red contours). All NMR experiments were, therefore, carried out at 40 °C. HMQC spectra of ILVM-labeled hTRF1 bound to either of U-^{2}H S210A DegP or U-^{2}H S210A Δloops DegP (Figure 3D middle and 3D right) established that much of the folded structure present in apo hTRF1 is lost upon binding, as the spectra resemble those obtained via thermal denaturation (compare Figure 3D middle, green contours, and right purple contours with Figure 3D left, red single contours). However, hTRF1 resonances from data sets recorded on either of the DegP complexes have better chemical shift dispersion than is the case for the thermally denatured apo client, potentially due to interactions in the complex, as observed in the cryo-EM model. In addition to peak shifts between bound and thermally unfolded free hTRF1 forms, we observed multiple bound state correlations for I30, V42, M43, and L44 that were not seen in data sets recorded on unbound hTRF1. Notably, I30 is located at the active site, with the other three residues situated in the bridging helix that connects regions of substrate that bind the PDZ1 and protease domains of DegP. Our data is, thus, consistent with multiple hTRF1 conformations in the bound state. As nearly identical spectra were observed for hTRF1 in complex with S210A DegP or S210A Δloops DegP, it is clear that the LA loops have little influence on the hTRF1 conformation, although minor chemical shift perturbations for L8 within the N-terminal half of hTRF1 were observed in a comparison of spectra recorded on the two cage forms (Figure 3D right), suggesting the possibility of weak interactions with the loops (see below).

https://doi.org/10.1021/jacs.3c13247
J. Am. Chem. Soc. 2024, 146, 8242−8259

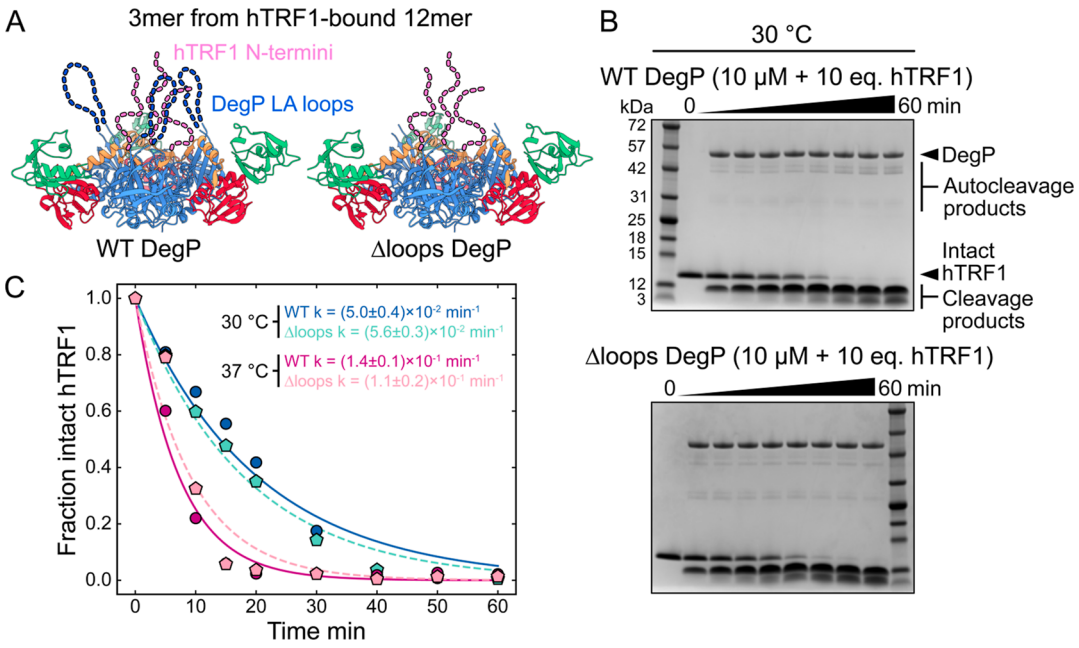

Figure 4. DegP LA loops have little influence on proteolysis rates of hTRF1. (A) Side views of a trimer from the hTRF1-bound 12mer structure (PDB 8F0U) highlighting that the disordered LA loops and the hTRF1 N-termini, both of which are not resolved in the model, can potentially interact to modulate proteolysis. The disordered LA loops of the protease domains are shown as dark blue dashed curves in wildtype DegP (WT, left) and are deleted in Δloops DegP (right). The hTRF1 N-termini are shown as pink dashed curves in each case. (B) Proteolytic activity assays via SDS PAGE measuring cleavage of intact hTRF1 (100 μM) by WT DegP (top) and Δloops DegP (bottom, each at 10 μM protomer concentration), 30 °C. The t = 0 point was obtained by preparing a separate sample of hTRF1 without DegP. Note that DegP undergoes slow autocleavage leading to degradation products with time. (C) Plots of the fraction of intact hTRF1 as a function of time for WT DegP (blue and red circles and lines) and Δloops DegP (green and pink pentagons and dashed lines) at 30 and 37 °C. The solid and dashed lines are the fits of an exponential decay function to each data set, with the associated decay constants (k) indicated in the top right corner of the plot.

Having established multiple conformations for the bound state, we next sought to probe conformational exchange on the millisecond time-scale by recording methyl-TROSY based ^{13}C-^{1}H Carr-Purcell-Meiboom-Gill (CPMG) relaxation dispersion experiments (Figure S2).[50] Figure 3E top plots ΔR_2 = $R_{2,\mathrm{eff}}$ (83.3 Hz) − $R_{2,\mathrm{eff}}$ (2000 Hz), the difference in effective transverse relaxation rates measured at the lowest and highest recorded CPMG frequencies ($\nu_{\mathrm{CPMG}} = 1/(4\delta)$, where 2δ is the time between successive ^{13}C refocusing pulses, Figure S2). The most significant values (>5 s^{-1}) are indicated as colored balls on the bound hTRF1 structure in Figure 3E bottom, including L8 and V19, and I30 and V42 in the N- and C-terminal halves of hTRF1, respectively. Dispersion profiles for these residues were well-described by a global two-state exchange model, with an exchange rate constant (k_{ex}) = 686 ± 142 s^{-1} and a minor state population (p_{B}) = 7.5 ± 1.1%, indicating that the bound hTRF1 chain interconverts between at least two conformations on a millisecond time scale. Notably, I30 and V42 (among other residues) also show multiple peaks in spectra (see above), suggesting dynamics on both ms and significantly slower time scales. Differences in ΔR_2 values were not observed in data sets recorded on cages with or without the LA loops, consistent with the LA loops having little influence on conformational excursions of the bound hTRF1 chain on the ms time scale (Figure S3). We have additionally probed faster (pico- to nanosecond) time scale methyl dynamics by recording the difference between methyl ^{1}H single-quantum fast and slow relaxation rates through measurement of the buildup of methyl proton triple-quantum coherence.[51] Fits of the buildup curves, as described in detail elsewhere,[51] allow the extraction of $S^2\tau_c$ values for methyl groups of hTRF1, where S^2 is a site-specific order parameter squared, related to the amplitude of motion of the methyl 3-fold axis, and τ_c is its effective tumbling time (Figure 3F; buildup curves for select residues are shown to the right and bottom of the correlation plot). Notably, the N-terminal methyl groups (pink in Figure 3F) are, in general, more flexible than those in the C-terminal half engaged by DegP (e.g., compare V19γ2 and V42γ2; note that Metε methyl groups are much more flexible on average relative to methyls of Leu, Val, or Ile,[64] giving rise to the small $S^2\tau_c$ values for M43ε despite its location in the C-terminal half of the client). In addition, $S^2\tau_c$ values were largest for the hTRF1 methyl probes localized to the protease and PDZ1 domain binding sites (e.g., I30δ1 and L54δ2). As described above, multiple peaks in methyl spectra are consistent with the bridging helix adopting several conformations. Notably, the low $S^2\tau_c$ value for M43ε, located in this bridging region, in particular relative to $S^2\tau_c$ for M51ε (in the PDZ1 binding site), shows that the bridging helix is flexible over a range of time scales, extending from ps−ns to seconds. Finally, the $S^2\tau_c$ values for N-terminal methyl groups of hTRF1 in the context of the S210A DegP cage are larger than for the S210A Δloops DegP cage (Figure 3F inset), consistent with client interactions with the LA loops that lead to a small but quantifiable restriction of the conformational freedom of the N-terminus of hTRF1 and, hence, to a reduction in ps−ns time scale motions in this region of the client.

3.3. Interactions between hTRF1 and the LA Loops Do Not Modulate Protease Activity. Given that our NMR-based analyses of the structural dynamics of hTRF1 within the 12mer cage suggested transient interactions between the N-terminal region of the client and the LA loops, we subsequently

https://doi.org/10.1021/jacs.3c13247
J. Am. Chem. Soc. 2024, 146, 8242−8259

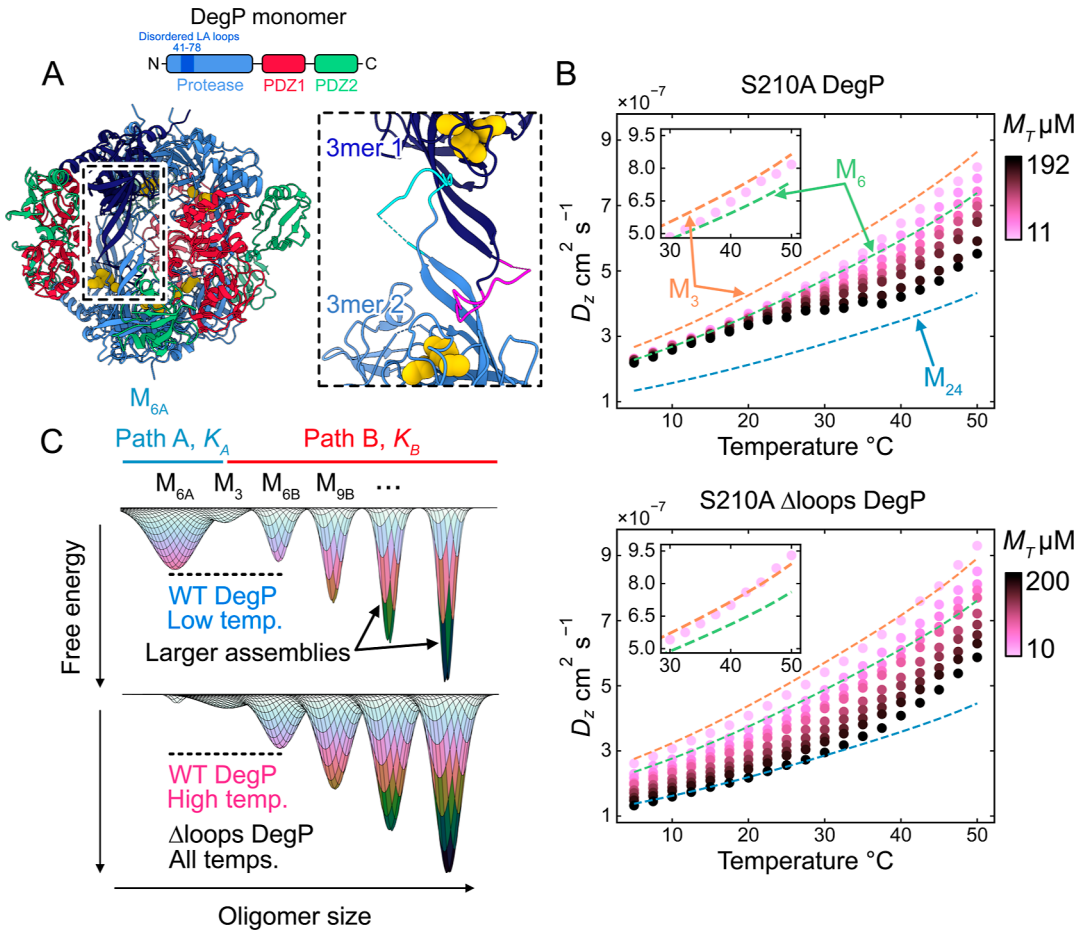

Figure 5. DegP protease domain LA loops regulate higher-order oligomerization. (A) Structure of apo M_{6A} (left, PDB 1KY9), stabilized by intertrimer β-strand and LA loop interactions (right, LA loop residues for the top and bottom protomers are colored magenta and cyan respectively; the remainder of the protease domains for the top and bottom protomer are colored navy and light blue, respectively). LA loops extend from the protease domain of each protomer within a given trimer into the active site (yellow) of a protomer from the opposing trimer. Note that the dashed lines indicate regions of the loops that are not observed, corresponding to 26 residues, i.e., the LA loops are much longer than depicted here. (B) DLS data sets for S210A[18] (top) and S210A Δloops (bottom) DegP, where D_z values have been measured as a function of temperature and the total DegP monomer concentration M_T. The dashed lines correspond to $D_0(T)$ for the 3mer, 6mer, and 24mer species calculated according to a scaling law that relates the diffusion constant to the number of trimers in each assembly, as shown in Figure 3C right. Note that an estimated trimer r_h of 4.75 nm for S210A Δloops DegP was used owing to its smaller hydrodynamic size compared to S210A DegP (r_h = 4.9 nm). The insets highlight the region of the data sets from 30 to 50 °C at the lowest monomer concentration (11 and 10 μM). (C) Free energy landscapes for WT (top) and Δloops (bottom) DegP in the absence of client proteins. The landscapes contain many wells of relatively similar energies, giving rise to a broadly populated distribution of species at physiological temperatures (~30−40 °C) and monomer concentrations (~100−200 μM). The oligomeric species involved in each of the two DegP self-assembly pathways (paths A and B) are indicated above the top energy landscape. To visualize these surfaces, we have assumed that the wells are represented by two-dimensional Gaussian functions. The trimer free energy was set as the reference point in each case, and the relative heights of the wells were calculated from ΔG values for path A and path B, as described previously.[18] Note the lower population of M_{6A} in Δloops DegP allows oligomerization to occur much more readily. The fractional population of each type of DegP oligomer is given by a combination of the depth and width of its associated energy well; wells with greater depths and widths accommodate larger numbers of particles.

examined whether such contacts have any effect on the proteolysis of hTRF1 in the context of an active DegP complex. Figure 4 illustrates a series of SDS PAGE-based proteolysis assays in which we compared the kinetics of hTRF1 cleavage by either DegP or Δloops DegP (Figure 4A). We initially used a biologically relevant DegP concentration of 10 μM[18] (protomer concentration) along with a 10-fold excess of hTRF1 to ensure the formation of 12mer cages and performed the experiments at 30 and 37 °C (Figure 4B). No appreciable changes to the cleavage kinetics were observed upon removal of the LA loops, as is evident from a comparison of the decay of the band corresponding to intact hTRF1 in Figure 4B top and bottom, 30 °C. This is further captured in the decay profiles recorded at both 30 and 37 °C that were generated through integration of the intact hTRF1 band intensities (Figure 4C) and subsequently fit with exponential functions. The effective rate constants (k) so obtained were the same to within error. Thus, at least in the case of hTRF1, and at the relative concentrations of enzyme and client used in the assay, any interactions with the LA loops have little influence on proteolytic activity over a range of temperatures at which DegP would operate in the periplasm of human pathogens.

We next asked whether differences between DegP and Δloops DegP cleavage rates would be observed in cases where the enzyme may not be saturated with substrate initially, such as for an equimolar amount of client (1:1) (Figure S4). The

https://doi.org/10.1021/jacs.3c13247
J. Am. Chem. Soc. 2024, 146, 8242−8259

rapid consumption of hTRF1 at higher temperatures, combined with difficulties in visualizing the hTRF1 bands at low concentrations, necessitated modifications to our assay. First, we reduced the temperature to 4 °C to slow the proteolysis reaction. Second, we used an hTRF1 concentration of 30 μM to enable accurate quantification of the gel bands, and hence, increased the concentration of DegP to 30 μM to ensure a 1:1 molar ratio. Together, the reduction in temperature and the use of 30 μM concentrations of enzyme and client allowed quantification of most of the hTRF1 decay profile in a reasonable period of time (Figure S4A,B). In this case, we observed a small difference between the two constructs, with Δloops DegP consuming hTRF1 approximately 20% more slowly than WT DegP (Figure S4B). The small difference in cleavage rates may indicate that interaction with the LA loops slightly increases binding of hTRF1 to DegP (which would manifest more significantly at the 1:1 ratio); however, given the relatively high affinity of the client, it is not surprising that only a small effect is observed between the two forms of the enzyme. For other substrates with different interaction propensities, this may not be the case, leading to greater differences in activity than observed here.

3.4. LA Loops within the Protease Domains of DegP Regulate Assembly of Higher-Order Apo Oligomers. As the LA loops did not influence proteolytic cleavage of hTRF1, we wondered whether they might play an alternate functional role. Others have shown that a N45F mutation in the LA loops can promote the formation of cages in response to substrates[33] and that their truncation can produce a distribution of oligomers from trimers to 12mers.[65] The extensive loop−loop contacts stabilizing trimers in M_{6A} (Figure 5A) suggested to us that the LA loops might serve an even more important role in buffering the formation of preorganized apo oligomers extending well beyond 12mers in path B in the context of the bifurcated model of Figure 1A. In order to explore this possibility, we compared the apo self-assembly landscapes of S210A and S210A Δloops DegP constructs through measurement of *z*-average diffusion constants (D_z) extracted from DLS measurements (Figure 5B). D_z values are an average of the diffusion constants for each species in solution, weighted by their relative light scattering intensities. Consequently, they can be used to inform on biomolecular self-assembly and binding interactions.[66,67] For example, we have recently shown that transformations of the oligomeric ensemble of DegP in response to mutations or changes in solution conditions such as salt concentration, temperature, and exposure to clients can be observed through variations in D_z values.[18,31]

To map out the influence of the LA loops on the oligomeric landscape of apo DegP, we collected DLS data sets where D_z values for both S210A DegP and S210A Δloops DegP were obtained as a function of temperature and total monomer concentration, M_T (Figure 5B). We simulated temperature-dependent diffusion constants for trimer, hexamer (M_{6A}), and 24mer particles, as described previously,[18] and overlaid these with the experimental data (shown as colored dashed lines in Figure 5B). Considering the S210A DegP data set (Figure 5B, top) first, a number of key insights into the apo ensemble and its redistribution in response to changes in temperature and M_T could immediately be obtained through qualitative analyses of the D_z values. First, at low temperatures (∼5−20 °C) and for all tested concentrations, the apo landscape is dominated by M_{6A}, as established by the agreement between the data and the hexamer diffusion constant under these conditions (i.e., the green line goes through the data). Second, at higher temperatures (∼20−50 °C) and low protein concentration (∼10 μM), M_{6A} dissociates into trimers, as illustrated by the transition of the D_z values toward the line corresponding to the diffusion constants of the trimer (Figure 5B top, inset). Third, as the protein concentration increases (>∼30 μM) and the temperature is elevated from ∼20 to 50 °C, the D_z values deflect below the profile for M_{6A} and approach the curve for the 24mer. This results from the assembly of higher order apo oligomers along path B through reorganization of the trimers. Fourth, over the range of ∼40−50 °C in this elevated concentration regime, the D_z values begin to increase, consistent with a weakening of interactions within the higher-order oligomers that leads to their depolymerization. The DLS data set for S210A Δloops DegP, in contrast, suggests a different rearrangement of oligomeric structures with temperature and concentration (Figure 5B bottom). The D_z values in the region of ∼5−25 °C and for M_T = 10 μM were consistent with a dramatic destabilization of M_{6A} (essentially no hexamer is observed) leading to a predominant population of trimers, as can be seen by the coincidence of the measured D_z values with those predicted for the trimeric DegP particle. At elevated temperatures (∼45−50 °C) and M_T = 10 μM, the measured diffusion constants transition slightly above the expected values for the trimer, consistent with the formation of smaller species (Figure 5B bottom, inset). The most striking differences between the S210A Δloops and S210A DegP profiles, however, were evident at lower temperatures and higher protein concentrations (∼5−30 °C and >10 μM), where D_z values for the S210A Δloops DegP decrease in proportion to M_T, while there is little change for S210A DegP. Notably, the two data sets are similar at higher temperatures and concentrations (∼35−50 °C and ∼30−200 μM).

The diffusion data provide key insights into the free energy landscapes of S210A and S210A Δloops DegP, highlighting an important role for the LA loops. As described previously,[18] the temperature and M_T dependent DegP DLS data could be explained by a bifurcated model involving paths A and B (Figures 1A and 5C), the latter path associated with the formation of larger oligomers. In this context, M_{6A} plays a critical gatekeeper role in controlling the relative importance of the two pathways: high concentrations of M_{6A} (at lower temperatures) shift the equilibrium toward path A, with depletion of M_{6A}, which occurs at higher temperatures, increasing the concentration of trimer particles that are available for subsequent formation of oligomers. This is illustrated in Figure 5C, where a simplified energy landscape of S210A DegP is shown for low and high temperatures. Similar landscapes were presented previously[18] but are reintroduced here to clarify the differences introduced by the LA loop-less variant studied presently. In the case of S210A DegP, the energy well for M_{6A} is below both the trimer and M_{6B} wells at low temperatures (Figure 5C top), leading to the observed paucity of path B oligomers (the well depths and widths are, respectively, the free energies of forming a given oligomer and measures of their population; deep and wide wells are more populated with their associated particles). At high temperatures, the M_{6A} well becomes shallow, shifting the path A equilibrium from M_{6A} to trimers which then readily associate into path B oligomers (Figure 5C bottom). The DLS data for S210A Δloops DegP show a wide distribution of D_z values at all temperatures, indicating significant populations of large oligomers, and hence a bifurcated pathway shifted to path B,

https://doi.org/10.1021/jacs.3c13247
J. Am. Chem. Soc. 2024, 146, 8242−8259

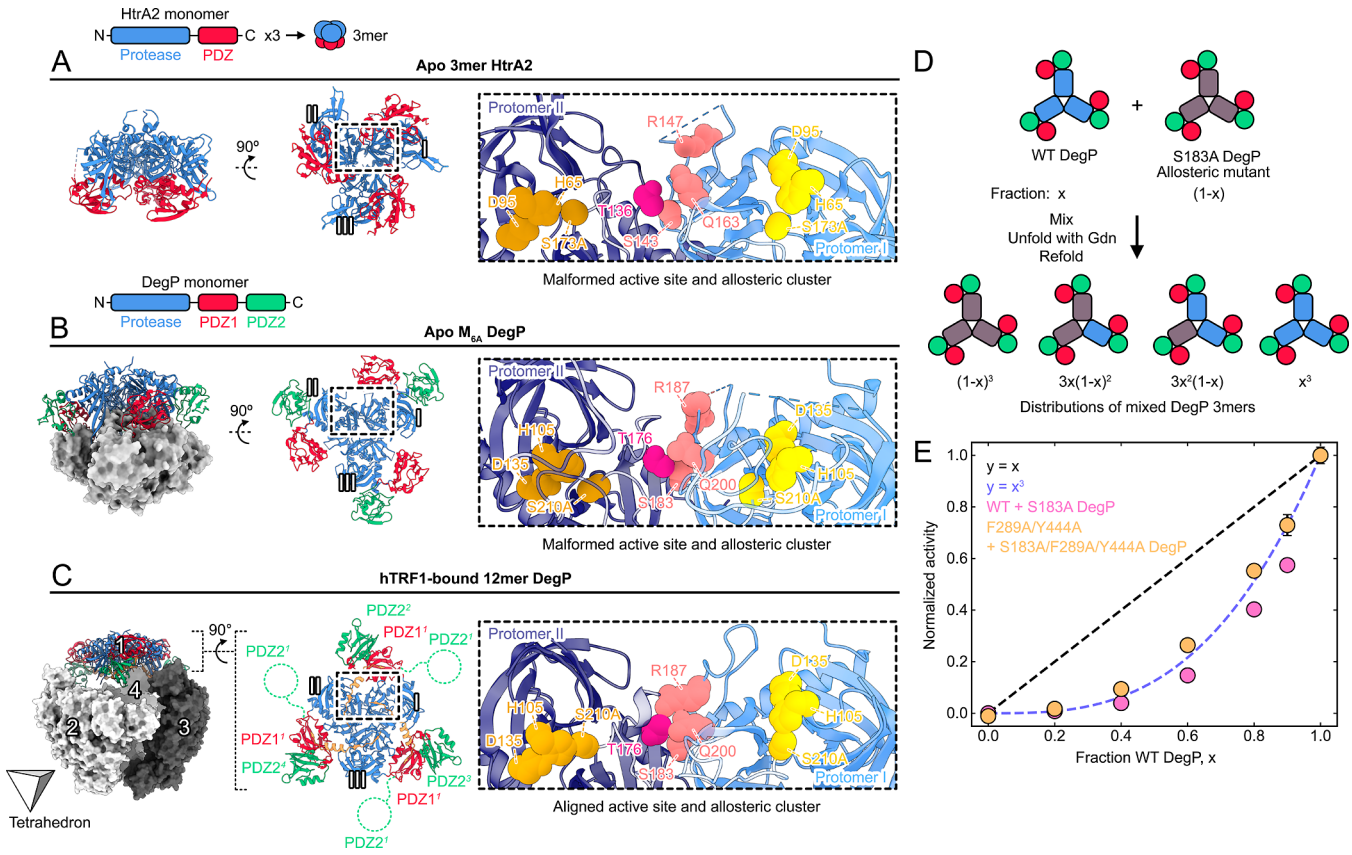

Figure 6. A concerted structural transition leads to activation of DegP. (A) Structure of the inactive, apo HtrA2 trimer (left, PDB 1LCY) shown in side and bottom views with the monomer domain architecture displayed above. The dashed black box overlaid on the bottom view of the structure outlines the protomer I:protomer II interface (right, the protease domains of protomer I and II are colored light and dark, respectively, to better delineate the interface). The active site catalytic triad is shown as yellow and dark yellow balls for protomers I and II respectively. Residues in HtrA2 that are equivalent to those in DegP involved in interprotomer communication leading to enzyme activation[69] are shown in pink in protomer I and magenta in protomer II. (B) Structure of apo M_{6A} DegP (left, PDB 1KY9), an inactive hexamer, shown in an analogous manner to the HtrA2 trimer in (A) with a closeup of key active site and allosteric residues (right) involved in proteolytic activation. (C) Structure of the hTRF1-bound DegP 12mer (left, PDB 8F0U) shown in the same manner as (A,B), with active site and allosteric residues that are crucial to proteolysis highlighted (right). (D) Schematic depicting the strategy for preparing mixed protomer DegP samples for fluorescence-based peptidase assays. The WT and S183A allosteric mutant versions of DegP trimers are shown with their protease domains colored blue and brown, respectively (top). Mixing of the WT and mutant DegP protomers in ratios of x:$(1 - x)$ leads to the formation of four different types of DegP trimers (bottom), with fractional populations as indicated. Note that only one of three rotationally symmetric conformations of the mixed trimers is displayed. (E) Plot of normalized peptidase activity as a function of the fraction of WT DegP monomers (x). Pink and orange colored circles correspond to activities of mixed samples of WT and S183A (pink) or F289A/Y444A and S183A/F289A/Y444A (orange; the F289A/Y444A double mutant can only form trimers, while WT and S183A can form higher-order oligomers) DegP. The black and dark blue dashed lines are models of DegP activity which respectively assume that the protease domains activate independently (noncooperative, $y = x$), or that a concerted structural transition is required for activation involving all three protomers of a trimer (total positive cooperativity, $y = x^3$). Error bars are one standard deviation based on triplicate measurements.

throughout the complete temperature range, as observed for S210A DegP only at high temperatures. The energy landscape for S210A Δloops DegP (Figure 5C bottom) is, therefore, only weakly temperature dependent, with M_{6A} assembly never more favorable than the formation of path B oligomers (i.e., only very small concentrations of M_{6A} are present under all conditions). Moreover, the similar DLS profiles for both DegP constructs at high temperatures strongly suggest that the $PDZ1^i$:$PDZ2^j$ interactions that play a significant role in stabilizing oligomers along path B[18] (e.g., see structure of client bound 12mer in Figure 1B) are unperturbed by deletion of the LA loops, lending further support to the notion that the loops primarily modulate the relative stabilities of M_{6A} and M_3 and not interactions within other parts of the cage.

3.5. A Concerted Structural Transition of the Protease Domains Underlies DegP Activation. Although functional interactions between hTRF1 and the LA loops within the central region of the 12mer cage could not be detected, the loops, nevertheless, are critical for controlling the concentration of M_{6A} that, in turn, regulates formation of apo, oligomeric DegP structures. In an effort to better understand the determinants of client proteolysis, we focused on interactions within the protease domain cores in anticipation that these might regulate activity. Sauer and co-workers have established that a conserved cluster of residues localized to the interprotease surfaces is required for communication between protomers in DegS and DegP[68] and recently we have shown that a similar scenario holds for the related HtrA2 protease from the human mitochondrial inner membrane space (Figure 6A).[69] In addition, our NMR studies of HtrA2 established that a concerted transition involving all three protomers of the trimeric HtrA2 structure must occur prior to activation, and

https://doi.org/10.1021/jacs.3c13247
J. Am. Chem. Soc. 2024, 146, 8242−8259

only when all binding sites are saturated. We wondered whether a similar concerted transition of trimer building blocks in DegP cages would be required for activity in this enzyme as well.

DegP and HtrA2 share common structural features but also display significant differences. For example, the DegP and HtrA2 trimers are arranged differently, with the single PDZ domain of an HtrA2 protomer covering the catalytic site of its protease domain, forming an overall trimer architecture that resembles a pyramid structure[70] (Figure 6A left and center). In contrast, the trimer building blocks in DegP are "flatter" with the PDZ domains extending outward from the protease domains so that the catalytic sites become exposed (Figure 6B,C left and center);[29] these are sequestered in M_{6A} by the long LA loops from the adjacent trimer in the hexameric structure,[10] while in the case of larger oligomers, they are localized inside the cavities that the complexes form.[28] Despite the differences in global structural features, there are striking similarities at the level of the interprotomer interfaces (Figure 6A−C right). First, in trimers from both M_{6A} and the hTRF1-bound 12mer, the same sets of residues (T176, S183, R187, and Q200) as in HtrA2 (T136, S143, R147, and Q163) are localized to the interfaces. Note that the HtrA2 sequence has been renumbered here for comparison with DegP by subtracting the length of the N-terminal region of the proenzyme that is removed, with the residue numbering in prior publications obtained by adding 133.[69,71] Second, in M_{6A}, the set of residues listed above are in a similar catalytically misaligned conformation as for apo HtrA2 (compare Figure 6A right and 6B right). Third, these residues are reorganized in the client-bound 12mer structure and become more closely packed, facilitated by the ordering of the L3 loop containing R187 and the shift of the loops adjoining the active sites into the "open" conformation (compare Figure 6B right and 6C right).[31] Similarly, the interprotomer interface in HtrA2 is also rearranged upon substrate binding, as observed in NMR studies.[69]

In order to establish whether an interprotomer communication network exists in DegP that functions in a concerted manner, as has previously been shown for HtrA2,[69] we generated a set of samples where WT and S183A DegP trimers were mixed in various ratios (Figure 6D top) and their peptidase activity was analyzed. The choice of the S183A mutation was motivated by our studies of HtrA2, where the related S143C-substitution was shown to disrupt the network required for interprotomer communication, preventing the concerted conformational change of the protease domains that enables proteolysis. Notably, in this case, even a single S143C protomer was sufficient to deactivate the enzyme. Random mixing, as established previously in HtrA2 mixing experiments,[69] leads to the assembly of four unique types of trimers, each of which has a different protomeric composition (i.e., 0, 1, 2, or 3 WT monomers), as shown in Figure 6D (bottom) with the relative fractions of the four trimers indicated. In order to ensure that the addition of S183A protomers had little influence on the apo cage distributions that are formed, we carried out a series of DLS control experiments as a function of temperature and M_T on a sample of the S183A mutant, as well as on a sample of S183A/F289A/Y444A DegP that only forms trimers (see below). Notably, the S183A substitution did not affect the DegP oligomers (Figure S5).

The peptidase activity profile obtained as a function of the fraction of WT DegP protomers, normalized to the maximum rate of cleavage ($x = 1$), is displayed in Figure 6E. The data were not consistent with a model whereby DegP protease domains undergo independent conformational changes to become active ($y = x$, where y is normalized activity, Figures 6E and S6). Poor fits were also obtained assuming a model where activation can occur when trimers contain either two or three WT protomers (Figure S6). However, the data (pink circles) were well fitted to a $y = x^3$ model, indicating that activity only occurs when all three protomers of a trimer building block are WT, as observed for HtrA2. We note that there was some deviation from $y = x^3$ for higher fractions of WT DegP ($x \sim 0.6-0.8$). We speculated that this results from communication between trimers in the large active oligomeric structures that form upon addition of substrate. In order to test this possibility, we repeated the experiments using an F289A/Y444A mutant of DegP which only forms trimers (i.e., cannot oligomerize). In this case, the normalized activity profile was well fitted by a cubic equation over the complete range of F289A/Y444A DegP fractions. Thus, activation of protease domains within each trimer only occurs when all protomers can undergo a concerted conformational change to an active conformation. Further, our data are consistent with cross-talk between trimer building blocks in oligomeric structures playing a role in proteolysis.

4. DISCUSSION AND CONCLUSIONS

DegP is a key protease involved in the maintenance of periplasmic protein homeostasis and bacterial virulence.[24] An understanding of the DegP conformational landscape and how it is remodeled by effectors is a necessary step toward the rational design of novel antibiotics for reducing Gram-negative bacterial pathogenicity.[32] Despite the abundance of clients with folded structures in the periplasm, little is known about how they interact with DegP. Insight into the binding mechanisms of folded clients, their structural dynamics in the DegP bound state, and how these relate to assembly and proteolysis, is therefore of interest.

In this study, we have addressed how a model folded client influences the activation cycle of DegP using a combination of hydrodynamics, solution NMR, and proteolysis measurements. We have established that (i) 12mer cage formation in response to hTRF1 binding occurs with positive cooperativity, (ii) the bound form of hTRF1 is dynamic over a range of time scales and the effects of the LA loops on these dynamics are modest, (iii) the LA loops serve as regulatory structural elements controlling the stability of M_{6A} which, in turn, modulates the higher-order assembly landscape, with little effect on hTRF1 proteolysis rates at 1:1 or 1:10 enzyme to client ratios, and, finally, that (iv) a concerted conformational change of the protease domains of DegP must occur prior to client proteolysis. It is noteworthy that hTRF1 proteolysis rates at 30 and 37 °C (1:10 DegP:hTRF1) were unchanged in cages lacking the LA loops, despite the fact that the distribution of apo oligomeric DegP structures is affected by these loops, although under the conditions of our assays, the major differences are primarily associated with the populations of M_{6A} and 3mer and not with higher order oligomers. In addition, only a small change in cleavage rates was observed using a 1:1 ratio of DegP to client at 4 °C, where the relative stability of M_{6A} in DegP is much higher than in Δloops DegP. This further emphasizes the highly cooperative nature of hTRF1 binding (Figure 1C,D) causing a rapid shift to the 12mer state, independent of the initial apo oligomer

https://doi.org/10.1021/jacs.3c13247
J. Am. Chem. Soc. 2024, 146, 8242−8259

distribution. It will be of interest to establish whether this is also the case for other substrates, in particular for those where binding might be less cooperative or weaker than for hTRF1.

Our studies demonstrating cooperative cage formation in the presence of hTRF1 are in agreement with earlier investigations using short disordered peptides as simplified models of clients.[29,72] The rearrangement of DegP upon hTRF1 binding is presumably facilitated by the two-pronged, simultaneous interaction of the client C-terminal region with the protease and PDZ1 binding sites, whereby the linkage of PDZ1 and protease domain binding motifs drives formation of the active complex, as discussed previously.[29] The client−host interactions so formed lead to a concentration dependence of cage formation which enables DegP to be relatively dormant under low substrate loads and to rapidly assemble into cages as required during aberrantly elevated substrate levels. Our studies further establish the importance of going beyond a single structure description of DegP cages to include the significant role of structural heterogeneity in function. Although a single pose was observed for the C-terminal region of hTRF1 in DegP 12mers in our recent cryo-EM study, proteolysis studies by our group measuring products of a series of clients by mass spectrometry provided strong evidence of multiple substrate binding modes in the catalytic sites of the enzyme.[31] The presence of multiple peaks in spectra for methyl group probes attached to regions of hTRF1 close to the site of cleavage and in the bridging helix connecting the PDZ1 and protease domains of DegP provides further evidence of the multiplicity of substrate−cage interactions that regulate function.

The work presented adds to a growing body of evidence in support of the critical role of IDRs of proteins in regulating important functional aspects of otherwise well-folded molecules.[73,74] In the case of DegP, we show that the LA loops are gatekeepers for the flow of trimers between two bifurcated pathways controlling the concentration of oligomers that are, in turn, responsible for client binding and processing. Notably, in the absence of the LA loops, the oligomerization reaction resembles one of isodesmic polymerization in which assembly proceeds in proportion to the total amount of available subunits via one pathway.[75] As the LA loops vary in length and sequence between different bacterial species, it may be that they have evolved for specific growth conditions and stress responses. Further, it remains to be seen whether the corresponding loops in other bacterial species might interact more significantly with substrates, compared to hTRF1 and the *E. coli* DegP investigated here, and how these interactions might be influenced by different client structural propensities, such as for the predominantly β-strand PapA pilin monomer.[76] A further open question relates to whether client−loop interactions might modulate the chaperone/protease duality that is prevalent in many members of the HtrA family. Other important examples where partnership of disordered and structured elements is paramount for the regulation of protein self-assembly in bacteria include the cell division protein FtsZ, where a C-terminal tail controls binding of adapters and filament formation by its N-terminal folded subdomains,[77] and the dodecameric stress-response protein Dps, which protectively condenses DNA around its rigidified core through flexible N-terminal segments under conditions were oxidative damage could otherwise prevail.[78] The combination of disordered loops, flexible interdomain linkers, and oligomerization domains found in DegP and in other bacterial assemblies appears to be widely implemented to generate the structural heterogeneity and multivalency that are required for the function of many large bacterial proteins.

Cooperativity in biomolecular interactions is a pervasive regulatory phenomenon.[79,80] In the case of DegP, our data support a model of activation in which three levels of positive cooperativity exist. In the first level, cages can form without saturation of their constituent trimers with substrate, with bound protomers communicating their ligation status to neighboring unligated protomers to enable them to adopt a conformation that is assembly competent. Combined with the accumulation of favorable interfacial contacts between hTRF1-bound trimers as assembly proceeds, completed 12mers are favored relative to partially formed intermediates as in the cooperative assembly of other types of protein cages.[59] In the second level, a concerted structural transition of all protease domains within a trimer building block is required for a proteolytically active conformation. This step may well be conserved within the HtrA protein family, as it also occurs in the related HtrA2 protease.[69] Notably, the strict requirement for a concerted structural change involving all three protomers within the trimer and potentially saturation of the trimers within cages to achieve a proteolytically active state may explain how DegP can act as both a chaperone and a protease[9] since partly ligated trimers within the context of large cages could bind clients but would not be able to cleave them. Finally, fully bound, active trimers communicate their status to other trimers within the cage, further enhancing client cleavage. Collectively, our biophysical studies of DegP paint a picture of a highly dynamic and cooperative molecular machine whose energy landscape rapidly adapts to stresses within the cell.

■ ASSOCIATED CONTENT

Supporting Information

The Supporting Information is available free of charge at https://pubs.acs.org/doi/10.1021/jacs.3c13247.

Additional AUC, NMR, proteolytic activity, and DLS analyses (PDF)

■ AUTHOR INFORMATION

Corresponding Authors

Robert W. Harkness − *Department of Biochemistry, University of Toronto, Toronto M5S 1A8, Canada; Department of Molecular Genetics, University of Toronto, Toronto M5S 1A8, Canada; Department of Chemistry, University of Toronto, Toronto M5S 3H6, Canada; Program in Molecular Medicine, The Hospital for Sick Children Research Institute, Toronto M5G 0A4, Canada;* Email: r.harkness@utoronto.ca

Lewis E. Kay − *Department of Biochemistry, University of Toronto, Toronto M5S 1A8, Canada; Department of Molecular Genetics, University of Toronto, Toronto M5S 1A8, Canada; Department of Chemistry, University of Toronto, Toronto M5S 3H6, Canada; Program in Molecular Medicine, The Hospital for Sick Children Research Institute, Toronto M5G 0A4, Canada;* orcid.org/0000-0002-4054-4083; Email: lewis.kay@utoronto.ca

Authors

Huaying Zhao − *Laboratory of Dynamics of Macromolecular Assembly, National Institute of Biomedical Imaging and*

https://doi.org/10.1021/jacs.3c13247
J. Am. Chem. Soc. 2024, 146, 8242−8259

Bioengineering, National Institutes of Health, Bethesda, Maryland 20892, United States

Yuki Toyama − *Department of Biochemistry, University of Toronto, Toronto M5S 1A8, Canada; Department of Molecular Genetics, University of Toronto, Toronto M5S 1A8, Canada; Department of Chemistry, University of Toronto, Toronto M5S 3H6, Canada; Program in Molecular Medicine, The Hospital for Sick Children Research Institute, Toronto M5G 0A4, Canada;* Present Address: Center for Biosystems Dynamics Research, RIKEN, Kanagawa 230-0045, Japan

Peter Schuck − *Laboratory of Dynamics of Macromolecular Assembly, National Institute of Biomedical Imaging and Bioengineering, National Institutes of Health, Bethesda, Maryland 20892, United States;* orcid.org/0000-0002-8859-6966

Complete contact information is available at: https://pubs.acs.org/10.1021/jacs.3c13247

Notes

The authors declare no competing financial interest.

■ ACKNOWLEDGMENTS

This research was funded by grants from the Canadian Institutes of Health Research (CIHR), FDN-503573, the Natural Sciences and Engineering Research Council of Canada, FDN-455908 (L.E.K.), and supported by the Intramural Research Programs of the National Institute for Biomedical Imaging and Bioengineering, National Institutes of Health, Bethesda (P.S.). R.W.H. is grateful to CIHR and to the Hospital for Sick Children Research Institute for postdoctoral and Restracomp fellowships, respectively. Y.T. was supported through a Japan Society for the Promotion of Science Overseas Research Fellowship, an Uehara Memorial Foundation postdoctoral fellowship, and a fellowship from CIHR.

■ REFERENCES

(1) Olivares, A. O.; Baker, T. A.; Sauer, R. T. Mechanistic Insights into Bacterial AAA+ Proteases and Protein-Remodelling Machines. *Nat. Rev. Microbiol.* **2016**, *14* (1), 33−44.

(2) Saibil, H. Chaperone Machines for Protein Folding, Unfolding and Disaggregation. *Nat. Rev. Mol. Cell Biol.* **2013**, *14* (10), 630−642.

(3) Clerico, E. M.; Tilitsky, J. M.; Meng, W.; Gierasch, L. M. How Hsp70 Molecular Machines Interact with Their Substrates to Mediate Diverse Physiological Functions. *J. Mol. Biol.* **2015**, *427* (7), 1575−1588.

(4) Abayev-Avraham, M.; Salzberg, Y.; Gliksberg, D.; Oren-Suissa, M.; Rosenzweig, R. DNAJB6Mutants Display Toxic Gain of Function through Unregulated Interaction with Hsp70 Chaperones. *Nat. Commun.* **2023**, *14* (1), 7066.

(5) He, D.; Zhang, M.; Liu, S.; Xie, X.; Chen, P. R. Protease-Mediated Protein Quality Control for Bacterial Acid Resistance. *Cell Chem. Biol.* **2019**, *26* (1), 144−150.e3.

(6) Hsu, H.-C.; Wang, M.; Kovach, A.; Darwin, A. J.; Li, H. Pseudomonas Aeruginosa C-Terminal Processing Protease CtpA Assembles into a Hexameric Structure That Requires Activation by a Spiral-Shaped Lipoprotein-Binding Partner. *mBio* **2022**, *13* (1), No. e0368021.

(7) Schramm, F. D.; Schroeder, K.; Jonas, K. Protein Aggregation in Bacteria. *FEMS Microbiol. Rev.* **2020**, *44* (1), 54−72.

(8) Maisonneuve, E.; Ezraty, B.; Dukan, S. Protein Aggregates: An Aging Factor Involved in Cell Death. *J. Bacteriol.* **2008**, *190* (18), 6070−6075.

(9) Spiess, C.; Beil, A.; Ehrmann, M. A Temperature-Dependent Switch from Chaperone to Protease in a Widely Conserved Heat Shock Protein. *Cell* **1999**, *97* (3), 339−347.

(10) Krojer, T.; Garrido-Franco, M.; Huber, R.; Ehrmann, M.; Clausen, T. Crystal Structure of DegP (HtrA) Reveals a New Protease-Chaperone Machine. *Nature* **2002**, *416* (6879), 455−459.

(11) Pallen, M. J.; Wren, B. W. The HtrA Family of Serine Proteases. *Mol. Microbiol.* **1997**, *26* (2), 209−221.

(12) Chien, J.; Ota, T.; Aletti, G.; Shridhar, R.; Boccellino, M.; Quagliuolo, L.; Baldi, A.; Shridhar, V. Serine Protease HtrA1 Associates with Microtubules and Inhibits Cell Migration. *Mol. Cell. Biol.* **2009**, *29* (15), 4177−4187.

(13) Kuninaka, S.; Iida, S.-I.; Hara, T.; Nomura, M.; Naoe, H.; Morisaki, T.; Nitta, M.; Arima, Y.; Mimori, T.; Yonehara, S.; Saya, H. Serine Protease Omi/HtrA2 Targets WARTS Kinase to Control Cell Proliferation. *Oncogene* **2007**, *26* (17), 2395−2406.

(14) Suzuki, Y.; Imai, Y.; Nakayama, H.; Takahashi, K.; Takio, K.; Takahashi, R. A Serine Protease, HtrA2, Is Released from the Mitochondria and Interacts with XIAP, Inducing Cell Death. *Mol. Cell* **2001**, *8* (3), 613−621.

(15) Strauch, K. L.; Beckwith, J. An Escherichia Coli Mutation Preventing Degradation of Abnormal Periplasmic Proteins. *Proc. Natl. Acad. Sci. U.S.A.* **1988**, *85* (5), 1576−1580.

(16) Lipinska, B.; Zylicz, M.; Georgopoulos, C. The HtrA (DegP) Protein, Essential for Escherichia Coli Survival at High Temperatures, Is an Endopeptidase. *J. Bacteriol.* **1990**, *172* (4), 1791−1797.

(17) De Oliveira, D. M. P.; Forde, B. M.; Kidd, T. J.; Harris, P. N. A.; Schembri, M. A.; Beatson, S. A.; Paterson, D. L.; Walker, M. J. Antimicrobial Resistance in ESKAPE Pathogens. *Clin. Microbiol. Rev.* **2020**, *33* (3), No. e00181-19.

(18) Harkness, R. W.; Toyama, Y.; Ripstein, Z. A.; Zhao, H.; Sever, A. I. M.; Luan, Q.; Brady, J. P.; Clark, P. L.; Schuck, P.; Kay, L. E. Competing Stress-Dependent Oligomerization Pathways Regulate Self-Assembly of the Periplasmic Protease-Chaperone DegP. *Proc. Natl. Acad. Sci. U.S.A.* **2021**, *118* (32), No. e2109732118.

(19) Skórko-Glonek, J.; Zurawa, D.; Kuczwara, E.; Wozniak, M.; Wypych, Z.; Lipinska, B. The Escherichia Coli Heat Shock Protease HtrA Participates in Defense against Oxidative Stress. *Mol. Gen. Genet.* **1999**, *262* (2), 342−350.

(20) Leandro, M. R.; Vespoli, L. D. S.; Andrade, L. F.; Soares, F. S.; Boechat, A. L.; Pimentel, V. R.; Moreira, J. R.; Passamani, L. Z.; Silveira, V.; De Souza Filho, G. A. DegP Protease Is Essential for Tolerance to Salt Stress in the Plant Growth-Promoting Bacterium Gluconacetobacter Diazotrophicus PAL5. *Microbiol. Res.* **2021**, *243*, 126654.

(21) Lipinska, B.; Fayet, O.; Baird, L.; Georgopoulos, C. Identification, Characterization, and Mapping of the Escherichia Coli htrA Gene, Whose Product Is Essential for Bacterial Growth Only at Elevated Temperatures. *J. Bacteriol.* **1989**, *171* (3), 1574−1584.

(22) Braselmann, E.; Chaney, J. L.; Champion, M. M.; Clark, P. L. DegP Chaperone Suppresses Toxic Inner Membrane Translocation Intermediates. *PLoS One* **2016**, *11* (9), No. e0162922.

(23) Sklar, J. G.; Wu, T.; Kahne, D.; Silhavy, T. J. Defining the Roles of the Periplasmic Chaperones SurA, Skp, and DegP in *Escherichia Coli*. *Genes Dev.* **2007**, *21* (19), 2473−2484.

(24) Frees, D.; Brøndsted, L.; Ingmer, H. Bacterial Proteases and Virulence. In *Regulated Proteolysis in Microorganisms*; Dougan, D. A., Ed.; *Subcellular Biochemistry*; Springer Netherlands: Dordrecht, 2013; Vol. *66*, pp 161−192.

(25) Johnson, R. M.; Nash, Z. M.; Dedloff, M. R.; Shook, J. C.; Cotter, P. A. DegP Initiates Regulated Processing of Filamentous Hemagglutinin in Bordetella Bronchiseptica. *mBio* **2021**, *12* (3), No. e0146521.

(26) Ruiz-Perez, F.; Henderson, I. R.; Leyton, D. L.; Rossiter, A. E.; Zhang, Y.; Nataro, J. P. Roles of Periplasmic Chaperone Proteins in the Biogenesis of Serine Protease Autotransporters of *Enterobacteriaceae*. *J. Bacteriol.* **2009**, *191* (21), 6571−6583.

(27) Ge, X.; Wang, R.; Ma, J.; Liu, Y.; Ezemaduka, A. N.; Chen, P. R.; Fu, X.; Chang, Z. DegP Primarily Functions as a Protease for the Biogenesis of B-barrel Outer Membrane Proteins in the Gram-negative Bacterium *Escherichia Coli*. *FEBS J.* **2014**, *281* (4), 1226−1240.
(28) Krojer, T.; Sawa, J.; Schäfer, E.; Saibil, H. R.; Ehrmann, M.; Clausen, T. Structural Basis for the Regulated Protease and Chaperone Function of DegP. *Nature* **2008**, *453* (7197), 885−890.
(29) Kim, S.; Grant, R. A.; Sauer, R. T. Covalent Linkage of Distinct Substrate Degrons Controls Assembly and Disassembly of DegP Proteolytic Cages. *Cell* **2011**, *145* (1), 67−78.
(30) Jiang, J.; Zhang, X.; Chen, Y.; Wu, Y.; Zhou, Z. H.; Chang, Z.; Sui, S.-F. Activation of DegP Chaperone-Protease via Formation of Large Cage-like Oligomers upon Binding to Substrate Proteins. *Proc. Natl. Acad. Sci. U.S.A.* **2008**, *105* (33), 11939−11944.
(31) Harkness, R. W.; Ripstein, Z. A.; Di Trani, J. M.; Kay, L. E. Flexible Client-Dependent Cages in the Assembly Landscape of the Periplasmic Protease-Chaperone DegP. *J. Am. Chem. Soc.* **2023**, *145* (24), 13015−13026.
(32) Cho, H.; Choi, Y.; Min, K.; Son, J. B.; Park, H.; Lee, H. H.; Kim, S. Over-Activation of a Nonessential Bacterial Protease DegP as an Antibiotic Strategy. *Commun. Biol.* **2020**, *3* (1), 547.
(33) Krojer, T.; Sawa, J.; Huber, R.; Clausen, T. HtrA Proteases Have a Conserved Activation Mechanism That Can Be Triggered by Distinct Molecular Cues. *Nat. Struct. Mol. Biol.* **2010**, *17* (7), 844−852.
(34) Nishikawa, T.; Nagadoi, A.; Yoshimura, S.; Aimoto, S.; Nishimura, Y. Solution Structure of the DNA-Binding Domain of Human Telomeric Protein, hTRF1. *Structure* **1998**, *6* (8), 1057−1065.
(35) Tugarinov, V.; Kanelis, V.; Kay, L. E. Isotope Labeling Strategies for the Study of High-Molecular-Weight Proteins by Solution NMR Spectroscopy. *Nat. Protoc.* **2006**, *1* (2), 749−754.
(36) Gelis, I.; Bonvin, A. M. J. J.; Keramisanou, D.; Koukaki, M.; Gouridis, G.; Karamanou, S.; Economou, A.; Kalodimos, C. G. Structural Basis for Signal-Sequence Recognition by the Translocase Motor SecA as Determined by NMR. *Cell* **2007**, *131* (4), 756−769.
(37) Gans, P.; Hamelin, O.; Sounier, R.; Ayala, I.; Durá, M.; Amero, C. D.; Noirclerc-Savoye, M.; Franzetti, B.; Plevin, M. J.; Boisbouvier, J. Stereospecific Isotopic Labeling of Methyl Groups for NMR Spectroscopic Studies of High-Molecular-Weight Proteins. *Angew. Chem., Int. Ed.* **2010**, *49* (11), 1958−1962.
(38) Zhao, H.; Brautigam, C. A.; Ghirlando, R.; Schuck, P. Overview of Current Methods in Sedimentation Velocity and Sedimentation Equilibrium Analytical Ultracentrifugation. *Curr. Protoc. Protein Sci.* **2013**, *71* (1), 20.12.1−20.12.49.
(39) Zhao, H.; Li, W.; Chu, W.; Bollard, M.; Adão, R.; Schuck, P. Quantitative Analysis of Protein Self-Association by Sedimentation Velocity. *Curr. Protoc. Protein Sci.* **2020**, *101* (1), No. e109.
(40) Harding, S. E.; Johnson, P. The Concentration-Dependence of Macromolecular Parameters. *Biochem. J.* **1985**, *231* (3), 543−547.
(41) Laue, T. M.; Shah, B.; Ridgeway, T. M.; Pelletier, S. L. Computer-Aided Interpretation of Analytical Sedimentation Data for Proteins. *Analytical Ultracentrifugation in Biochemistry and Polymer Science*; Royal Society of Chemistry: Cambridge, UK, 1992.
(42) Brautigam, C. Calculations and Publication-Quality Illustrations for Analytical Ultracentrifugation Data. *Methods in Enzymology*; Academic Press, 2015; Vol. *562*, pp 109−133.
(43) Delaglio, F.; Grzesiek, S.; Vuister, G. W.; Zhu, G.; Pfeifer, J.; Bax, A. NMRPipe: A Multidimensional Spectral Processing System Based on UNIX Pipes. *J. Biomol. NMR* **1995**, *6* (3), 277−293.
(44) Lee, W.; Tonelli, M.; Markley, J. L. NMRFAM-SPARKY: Enhanced Software for Biomolecular NMR Spectroscopy. *Bioinformatics* **2015**, *31* (8), 1325−1327.
(45) Skinner, S. P.; Fogh, R. H.; Boucher, W.; Ragan, T. J.; Mureddu, L. G.; Vuister, G. W. CcpNmr AnalysisAssign: A Flexible Platform for Integrated NMR Analysis. *J. Biomol. NMR* **2016**, *66* (2), 111−124.
(46) Helmus, J. J.; Jaroniec, C. P. Nmrglue: An Open Source Python Package for the Analysis of Multidimensional NMR Data. *J. Biomol. NMR* **2013**, *55* (4), 355−367.
(47) Sattler, M. Heteronuclear Multidimensional NMR Experiments for the Structure Determination of Proteins in Solution Employing Pulsed Field Gradients. *Prog. Nucl. Magn. Reson. Spectrosc.* **1999**, *34* (2), 93−158.
(48) Tugarinov, V.; Hwang, P. M.; Ollerenshaw, J. E.; Kay, L. E. Cross-Correlated Relaxation Enhanced ^{1}H-^{13}C NMR Spectroscopy of Methyl Groups in Very High Molecular Weight Proteins and Protein Complexes. *J. Am. Chem. Soc.* **2003**, *125* (34), 10420−10428.
(49) Choy, W.-Y.; Mulder, F. A. A.; Crowhurst, K. A.; Muhandiram, D. R.; Millett, I. S.; Doniach, S.; Forman-Kay, J. D.; Kay, L. E. Distribution of Molecular Size within an Unfolded State Ensemble Using Small-Angle X-Ray Scattering and Pulse Field Gradient NMR Techniques. *J. Mol. Biol.* **2002**, *316* (1), 101−112.
(50) Korzhnev, D. M.; Kloiber, K.; Kanelis, V.; Tugarinov, V.; Kay, L. E. Probing Slow Dynamics in High Molecular Weight Proteins by Methyl-TROSY NMR Spectroscopy: Application to a 723-Residue Enzyme. *J. Am. Chem. Soc.* **2004**, *126* (12), 3964−3973.
(51) Sun, H.; Kay, L. E.; Tugarinov, V. An Optimized Relaxation-Based Coherence Transfer NMR Experiment for the Measurement of Side-Chain Order in Methyl-Protonated, Highly Deuterated Proteins. *J. Phys. Chem. B* **2011**, *115* (49), 14878−14884.
(52) Schindelin, J.; Arganda-Carreras, I.; Frise, E.; Kaynig, V.; Longair, M.; Pietzsch, T.; Preibisch, S.; Rueden, C.; Saalfeld, S.; Schmid, B.; Tinevez, J.-Y.; White, D. J.; Hartenstein, V.; Eliceiri, K.; Tomancak, P.; Cardona, A. Fiji: An Open-Source Platform for Biological-Image Analysis. *Nat. Methods* **2012**, *9* (7), 676−682.
(53) Koppel, D. E. Analysis of Macromolecular Polydispersity in Intensity Correlation Spectroscopy: The Method of Cumulants. *J. Chem. Phys.* **1972**, *57* (11), 4814−4820.
(54) Frisken, B. J. Revisiting the Method of Cumulants for the Analysis of Dynamic Light-Scattering Data. *Appl. Opt.* **2001**, *40* (24), 4087.
(55) Schuck, P. Size-Distribution Analysis of Macromolecules by Sedimentation Velocity Ultracentrifugation and Lamm Equation Modeling. *Biophys. J.* **2000**, *78* (3), 1606−1619.
(56) Batchelor, G. K. Brownian Diffusion of Particles with Hydrodynamic Interaction. *J. Fluid Mech.* **1976**, *74* (1), 1−29.
(57) Kops-Werkhoven, M. M.; Fijnaut, H. M. Dynamic Light Scattering and Sedimentation Experiments on Silica Dispersions at Finite Concentrations. *J. Chem. Phys.* **1981**, *74* (3), 1618−1625.
(58) Chaturvedi, S. K.; Sagar, V.; Zhao, H.; Wistow, G.; Schuck, P. Measuring Ultra-Weak Protein Self-Association by Non-Ideal Sedimentation Velocity. *J. Am. Chem. Soc.* **2019**, *141* (7), 2990−2996.
(59) Wargacki, A. J.; Wörner, T. P.; Van De Waterbeemd, M.; Ellis, D.; Heck, A. J. R.; King, N. P. Complete and Cooperative in Vitro Assembly of Computationally Designed Self-Assembling Protein Nanomaterials. *Nat. Commun.* **2021**, *12* (1), 883.
(60) Zlotnick, A. To Build a Virus Capsid: An Equilibrium Model of the Self Assembly of Polyhedral Protein Complexes. *J. Mol. Biol.* **1994**, *241* (1), 59−67.
(61) Ollerenshaw, J. E.; Tugarinov, V.; Kay, L. E. Methyl TROSY: Explanation and Experimental Verification. *Magn. Reson. Chem.* **2003**, *41* (10), 843−852.
(62) Stejskal, E. O.; Tanner, J. E. Spin Diffusion Measurements: Spin Echoes in the Presence of a Time-Dependent Field Gradient. *J. Chem. Phys.* **1965**, *42* (1), 288−292.
(63) Sekhar, A.; Rosenzweig, R.; Bouvignies, G.; Kay, L. E. Mapping the Conformation of a Client Protein through the Hsp70 Functional Cycle. *Proc. Natl. Acad. Sci. U.S.A.* **2015**, *112* (33), 10395−10400.
(64) Mittermaier, A.; Kay, L. E.; Forman-Kay, J. D. Analysis of Deuterium Relaxation-Derived Methyl Axis Order Parameters and Correlation with Local Structure. *J. Biomol. NMR* **1999**, *13*, 181−185.
(65) Jomaa, A.; Damjanovic, D.; Leong, V.; Ghirlando, R.; Iwanczyk, J.; Ortega, J. The Inner Cavity of *Escherichia Coli* DegP Protein Is Not Essentialfor Molecular Chaperone and Proteolytic Activity. *J. Bacteriol.* **2007**, *189* (3), 706−716.

https://doi.org/10.1021/jacs.3c13247
J. Am. Chem. Soc. 2024, 146, 8242−8259

(66) Hanlon, A. D.; Larkin, M. I.; Reddick, R. M. Free-Solution, Label-Free Protein-Protein Interactions Characterized by Dynamic Light Scattering. *Biophys. J.* **2010**, *98* (2), 297−304.
(67) Attri, A. K.; Fernández, C.; Minton, A. P. Self-Association of Zn-Insulin at Neutral pH: Investigation by Concentration Gradient-Static and Dynamic Light Scattering. *Biophys. Chem.* **2010**, *148* (1−3), 23−27.
(68) de Regt, A.; Kim, S.; Sohn, J.; Grant, R. A.; Baker, T. A.; Sauer, R. T. A Conserved Activation Cluster Is Required for Allosteric Communication in HtrA-Family Proteases. *Structure* **2015**, *23* (3), 517−526.
(69) Toyama, Y.; Harkness, R. W.; Kay, L. E. Dissecting the Role of Interprotomer Cooperativity in the Activation of Oligomeric High-Temperature Requirement A2 Protein. *Proc. Natl. Acad. Sci. U.S.A.* **2021**, *118* (35), No. e2111257118.
(70) Li, W.; Srinivasula, S. M.; Chai, J.; Li, P.; Wu, J.-W.; Zhang, Z.; Alnemri, E. S.; Shi, Y. Structural Insights into the Pro-Apoptotic Function of Mitochondrial Serine Protease HtrA2/Omi. *Nat. Struct. Biol.* **2002**, *9* (6), 436−441.
(71) Toyama, Y.; Harkness, R. W.; Lee, T. Y. T.; Maynes, J. T.; Kay, L. E. Oligomeric Assembly Regulating Mitochondrial HtrA2 Function as Examined by Methyl-TROSY NMR. *Proc. Natl. Acad. Sci. U.S.A.* **2021**, *118* (11), No. e2025022118.
(72) Thompson, N. J.; Merdanovic, M.; Ehrmann, M.; van Duijn, E.; Heck, A. J. R. Substrate Occupancy at the Onset of Oligomeric Transitions of DegP. *Structure* **2014**, *22* (2), 281−290.
(73) Brodsky, S.; Jana, T.; Mittelman, K.; Chapal, M.; Kumar, D. K.; Carmi, M.; Barkai, N. Intrinsically Disordered Regions Direct Transcription Factor In Vivo Binding Specificity. *Mol. Cell* **2020**, *79* (3), 459−471.e4. e4
(74) Wright, P. E.; Dyson, H. J. Intrinsically Disordered Proteins in Cellular Signalling and Regulation. *Nat. Rev. Mol. Cell Biol.* **2015**, *16* (1), 18−29.
(75) Van Der Zwaag, D.; Pieters, P. A.; Korevaar, P. A.; Markvoort, A. J.; Spiering, A. J. H.; De Greef, T. F. A.; Meijer, E. W. Kinetic Analysis as a Tool to Distinguish Pathway Complexity in Molecular Assembly: An Unexpected Outcome of Structures in Competition. *J. Am. Chem. Soc.* **2015**, *137* (39), 12677−12688.
(76) Jones, C. H.; Dexter, P.; Evans, A. K.; Liu, C.; Hultgren, S. J.; Hruby, D. E. *Escherichia Coli* DegP Protease Cleaves between Paired Hydrophobic Residues in a Natural Substrate: The PapA Pilin. *J. Bacteriol.* **2002**, *184* (20), 5762−5771.
(77) Shen, B.; Lutkenhaus, J. The Conserved C-terminal Tail of FtsZ Is Required for the Septal Localization and Division Inhibitory Activity of MinC ^{C}/MinD. *Mol. Microbiol.* **2009**, *72* (2), 410−424.
(78) Ceci, P.; Cellai, S.; Falvo, E.; Rivetti, C.; Rossi, G. L.; Chiancone, E. DNA Condensation and Self-Aggregation of Escherichia Coli Dps Are Coupled Phenomena Related to the Properties of the N-Terminus. *Nucleic Acids Res.* **2004**, *32* (19), 5935−5944.
(79) Freiburger, L.; Miletti, T.; Zhu, S.; Baettig, O.; Berghuis, A.; Auclair, K.; Mittermaier, A. Substrate-Dependent Switching of the Allosteric Binding Mechanism of a Dimeric Enzyme. *Nat. Chem. Biol.* **2014**, *10* (11), 937−942.
(80) Motlagh, H. N.; Wrabl, J. O.; Li, J.; Hilser, V. J. The Ensemble Nature of Allostery. *Nature* **2014**, *508* (7496), 331−339.
(81) Winkler, J. R. Numerical Recipes in C: The Art of Scientific Computing, Second Edition. *Endeavour* **1993**, *17* (4), 201.

https://doi.org/10.1021/jacs.3c13247
J. Am. Chem. Soc. 2024, 146, 8242−8259